

THESIS

TRENDS IN REGIONAL ATMOSPHERIC WATER CYCLES ACROSS OCEAN BASINS
DIAGNOSED USING MULTIPLE PRODUCTS

Submitted by

Drew W. Koeritzer

Department of Atmospheric Science

In partial fulfillment of the requirements

For the Degree of Master of Science

Colorado State University

Fort Collins, Colorado

Spring 2021

Master's Committee:

Advisor: Christian Kummerow

Christine Chiu
Jeffrey Niemann

Copyright by Drew W. Koeritzer 2021

All Rights Reserved

ABSTRACT

TRENDS IN REGIONAL ATMOSPHERIC WATER CYCLES ACROSS OCEAN BASINS DIAGNOSED USING MULTIPLE PRODUCTS

The importance of water within the earth system, especially its direct impacts on weather and climate through its presence and transport in the atmosphere, cannot be overstated. Accordingly, it is critical to obtain an accurate baseline understanding of the current state of the atmospheric branch of the water cycle if we are to infer future changes to the water cycle and associated influences on weather and climate. Technological advances in both remote and in-situ observing systems have made it possible to characterize water and energy budgets on global scales. However, relatively little work has been done to study the degree of closure, and thus the accuracy of these methods, at regional scales – especially over the oceans. This is a task complicated by the lack of long-term continuous data records of the variables of interest, including ocean surface evaporation, atmospheric water vapor flux divergence, and precipitation. This work aims to fill these gaps and contribute to the establishment of a baseline understanding of the water cycle within the current TRMM and GPM era.

The evolution of water cycle closure within five independent regions in the equatorial Pacific, Atlantic, and Indian Oceans has been established previously using atmospheric reanalysis and gridded observational and pseudo-observational data products. That research found that while the water budgets closed extremely well in most basins, the water cycle within the West Pacific was found to trend out of closure within the first decade of the 21st century. The current study aims to extend this analysis temporally, in addition to including a wider variety of

independent data sources to confirm the presence of this emerging lack of closure and hypothesize the reason for its existence. Differences between independent products are used within the context of each region to infer whether the emerging lack of closure is a data artifact or is a result of a more fundamental shift in the physical mechanisms and characteristics of the evaporation, precipitation, or water vapor flux divergence within a specific region.

Results confirm an initial hypothesis that the emerging lack of water cycle closure in the West Pacific is not due to satellite or instrument drift. Rather, it appears to be related to changes in the prevalence of deep isolated versus deep organized convection in the West Pacific region and its associated impact on passive microwave precipitation retrieval algorithms.

ACKNOWLEDGEMENTS

I would like to thank my advisor, Chris Kummerow, for his guidance and the time he spent mentoring me during my time at CSU. It has been an amazing experience to work with him and with the rest of the talented scientists in his research group. The advice I have received from Chris throughout this process has helped me grow as a scientist in more ways than I ever expected, and for that I am extremely thankful. Thank you to the other students in Chris' group, who encouraged me and helped me through the challenges of balancing coursework and research. It has been so much fun to work with each of you, and all of your perspectives have been enormously helpful and valuable to me. Thank you also to the CSU Department of Atmospheric Science as a whole, for being so welcoming and supportive. Lastly, I would like to thank my family and friends for their unwavering support, and for helping me make a career out of atmospheric science. I would not have been able to complete this work without them.

TABLE OF CONTENTS

ABSTRACT	ii
ACKNOWLEDGEMENTS.....	iv
CHAPTER 1: INTRODUCTION.....	1
CHAPTER 2: DATA AND BACKGROUND.....	10
2.1: EVAPORATION	10
2.2: PRECIPITATION	16
2.3: ATMOSPHERIC WATER VAPOR FLUX DIVERGENCE	24
CHAPTER 3: RESULTS AND ANALYSIS	27
3.1: EVAPORATION	28
3.2: PRECIPITATION	36
3.3: ATMOSPHERIC WATER VAPOR FLUX DIVERGENCE (DIVQ)	43
3.4: OVERALL MAGNITUDE OF WATER CYCLE CLOSURE	54
CHAPTER 4: DISCUSSION AND CONCLUSIONS.....	58
4.1: SUMMARY OF DIFFERENCES BETWEEN PRODUCTS.....	58
4.2: IMPLICATIONS ON MAGNITUDE OF CLOSURE	61
REFERENCES	70

CHAPTER 1: INTRODUCTION

Water, in all phases, is arguably the atmospheric constituent which is most influential on day-to-day life. As such, it is no wonder that of all atmospheric constituent gases, water has received the most scientific interest throughout the last century. Water is not uniformly mixed throughout the atmosphere, and its transport mechanisms were an early research focus because of connections to clouds and precipitation. This was greatly aided by the development and proliferation of meteorological satellites during the 1970s and the following decades. Some of the earliest studies to take advantage of new satellite technology focused on deducing atmospheric wind vectors from novel observations from geostationary satellites (e.g. Leese et al. 1971, Young et al. 1972, among others). This work, in combination with water vapor climatology and applications such as those from Rasmusson (1967, 1977) and others, in addition to the novel use of passive microwave observations to infer temperature, moisture, and precipitation (e.g. Wilheit et al. 1977, 1980) allowed for the rapid buildup of a broad comprehension of the state of the atmosphere, as well as the foundations for using ever-advancing remote sensing technology to improve this understanding.

While it was indeed this foundational early scientific work which established baseline understanding of the characteristics, patterns, and transport of atmospheric water vapor, later work has focused on understanding the presence of atmospheric water vapor as a component within the broader hydrologic cycle. This was manifested as a shift from thinking about the hydrologic cycle components of evaporation, precipitation, and atmospheric transport individually to considering them as part of an inseparable system. Chahine (1992) advocated this viewpoint, among others, emphasizing the importance of the role of water within the hydrologic

cycle in influencing the broader climate system. Even more recently, as the influences of global warming and climate change have become more apparent, several studies have sought to predict how the hydrologic cycle will respond to a warming climate. Most prolific in this regard is the work of Held and Soden (2006), which utilizes climate models to hypothesize likely changes in the hydrologic cycle based on model simulations. Simply put, this work stipulates that despite a lack of knowledge of the precise amount of warming that will occur, lower-tropospheric water vapor content will increase following the Clausius-Clapeyron relation, which tightly links it to surface temperature. This warming-induced increase in lower-tropospheric water vapor has several far-reaching consequences on the broader hydrologic cycle, including changes in mass and heat fluxes, as well as an increase in the temporal variability and magnitude of the balance between evaporation and precipitation (Held and Soden 2006), a quantity frequently utilized in studies characterizing the state of the balance of the hydrologic cycle.

As models and observations have advanced, it has become increasingly possible to quantify water and energy fluxes globally at multiple temporal scales. Globally, scientific understanding of the components of the energy and water cycles is fairly well-developed. Comprehensive characterizations of these fluxes have most recently been completed for the energy cycle by many well-regarded studies (e.g. Trenberth et al. 2009, Stephens et al. 2012, Wild et al. 2013, L'Ecuyer et al. 2015) and for the water cycle by Rodell et al. (2015). The stated motivation for these studies was to establish a baseline understanding of the water and energy budgets of the current Earth system, with an ultimate goal of obtaining a complete understanding of how climate change will affect this current state. While these studies represent a notable feat in that they are able to present a comprehensive view of the state of global water and energy cycles, they also note the importance of continuing to refine the models and improve the

accuracy and robustness of the observations used to derive the values present in their results. Namely, different observational sources produce different results, and both observations and models may be sensitive to regional variations in climatology and meteorology. Analysis of the atmospheric water budgets on regional scales has the potential to expose weaknesses in products describing the individual components of the water cycle which may be hidden when considered only at global scales. Additionally, studies of the components of the water cycle at regional scales allow for the identification of trends in water budget closure which may reveal changes in the local physical environment which in turn may lead to errors in observed or modeled products. Within this current era of a warming climate, research foci can primarily be divided into two separate areas; first, consideration of how warming affects the overall energy balance; and second, how individual components of the hydrologic cycle vary regionally and how this can provide insight into the broader trends in the overall cycle. It is this second area of focus which is the primary scope of this work.

The components of the atmospheric hydrologic cycle, including evaporation, precipitation, and water vapor flux divergence (hereafter referred to as $\text{div}Q$), are challenging to accurately and consistently observe over remote ocean regions, and a lack of a comprehensive in-situ observational record of all of these variables has made assessing the degree of closure of the water cycle quite difficult. In contrast to the temporal and spatial gaps present within many raw observational products depicting these variables, atmospheric reanalysis products are designed to be both temporally and spatially continuous, providing a picture of the state of the atmosphere at nearly any point at any time. Reanalyses have become a key part of climate and meteorological studies and have improved vastly in accuracy and resolution in recent iterations. Broadly speaking, an atmospheric reanalysis creates this continuous representation of the state of

the atmosphere by ingesting a large quantity of observations via a fixed data assimilation system, while relying on a numerical model to ensure that physical consistency is adhered to (Gelaro et al. 2017). Consequently, reanalyses embody the physics and limitations of the underlying numerical model.

Many of the meteorological centers operated by agencies around the world produce an atmospheric reanalysis product. Two prominent examples used here include the National Aeronautics and Space Administration (NASA) and the European Centre for Medium-Range Weather Forecasts (ECMWF) which produce the MERRA-2 and ERA-5 reanalysis products, respectively. While a brief description of these reanalyses is included here, the reader is encouraged to refer to the cited literature for more detailed information. ERA-5 is the latest in a long line of reanalysis products produced by ECMWF, which replaces the prior-generation ERA-Interim reanalysis (Dee et al. 2011) and improves temporal and spatial resolution as well as variable availability compared to earlier reanalyses (Hersbach and Dee 2017, Hersbach et al. 2020). MERRA-2 is an update to the original version of MERRA (Reinecker et al. 2011) intended to improve upon known deficiencies in MERRA, upgrade the underlying model, and incorporate the assimilation of new observational data types (Gelaro et al. 2017). Despite the advances of these most recent reanalysis products, both MERRA-2 and ERA-5 still suffer from the drawbacks typical of all reanalysis products. Most prominent of these is the dependence of the analysis output on the quality of the observations used as input to the data assimilation system. This is especially true for output in regions without consistent in-situ observations, such as over the oceans. In these sparsely-observed regions, reanalysis output depends heavily on evolving satellite observing systems. Nevertheless, modern reanalysis products serve as a useful comparison metric to purely observational products. Additionally, reanalysis depictions are often

the only available data for remote regions and therefore are tremendously valuable, as long as their limitations are considered within the interpretation of results. Because there are no direct observations of $\text{div}Q$, this study uses $\text{div}Q$ depictions exclusively from reanalysis products. While there are few direct three-dimensional measurements of wind, the fairly direct assimilation of water vapor, temperature, and atmospheric wind observations (Hersbach et al. 2020) provide some confidence in depiction of $\text{div}Q$.

Due to the drawbacks of reanalysis data, observations still play a critical role in characterizing the current state of the atmosphere and the climate system as a whole. However, observations are plagued by their own set of drawbacks, particularly related to long-term stability and temporal consistency. This lack of a consistent data record is a well-known problem within long-term studies of climate, as it makes it very difficult to distinguish between trends caused by changes in observing systems themselves and actual physical changes within the environment. A comparable situation is the difficulty of establishing a long-term record of atmospheric temperature using radiosondes. Sherwood et al. (2005) analyzed trends in temperatures measured by radiosondes. This revealed what appeared to be a trend towards cooler temperatures. However, further analysis revealed this to be a spurious trend caused by uncorrected error related to the instrument itself (Sherwood et al. 2005). Results such as these emphasize the importance of understanding all possible sources of error within a given measurement. When considering the individual components of the hydrologic cycle over oceans, direct observation of each component is not possible outside of very limited spatial or temporal periods which are often related to intensive field campaigns. As such, the advancement of spaceborne observing technologies has provided a viable alternative to direct observations in the form of remotely sensed observations from satellite-mounted instruments. Even with the wide availability of

observations, models and atmospheric reanalysis products are sometimes still used to fill in temporal gaps left by the lack of continuous temporal sampling which is a difficulty inherent to many satellite-based observational products.

Besides $\text{div}Q$, which as previously described is limited to depictions from reanalysis products, the two remaining variables in the atmospheric branch of the hydrologic cycle are evaporation and precipitation. Ocean surface evaporation can only be directly measured on very small scales, with anything larger generally requiring the use of bulk flux formulations which themselves require variables which cannot be fully observed. Original depictions of ocean surface fluxes were limited to those obtained through in situ field studies. The impactful limitations on both spatial and temporal resolution of this approach motivated an interest in the development of more continuous products utilizing satellite observations. Because of the wide interest in and applicability of ocean surface fluxes present across multiple disciplines, there have been several gridded observationally-based flux products developed in recent decades, in addition to reanalysis depictions of these same fluxes. Well-known among these are the SeaFlux product (Clayson et al. 2015), which is as close to purely observational as possible, and the OAFlux product, (Yu and Weller 2007) which optimally blends observations with reanalysis data. These gridded products, however, are not without limitations, and these and the construction methods of the algorithms will be described in a later section.

Spaceborne passive microwave-based retrievals of precipitation are broadly considered to be a robust method of estimating precipitation on large scales, especially over oceans. The legacy of these retrieval methods extends nearly to the advent of meteorological satellites themselves. Retrieval methods utilized early geostationary infrared observations to correlate cloud top temperature with rainfall before advancing to more advanced methods utilizing passive

microwave observations with the introduction of polar orbiting satellite systems. Through the evolution and refining of several generations, these passive microwave retrievals are well-regarded as the standard for remotely-sensed observations of precipitation, and are often the only product that is continuously available over remote regions. While these passive microwave products are better than their visible and infrared-based predecessors, they are limited to a narrow swath determined by the specific orbit of the satellite. To overcome this limitation, gridded products have been developed which blend passive microwave observations with geostationary visible and infrared data to obtain precipitation estimates which are continuous in space and time. Two well-known products include the Global Precipitation Climatology Project (GPCP) and the Integrated Multi-Satellite Retrievals for GPM (IMERG).

These products and their limitations will be discussed in detail in a later section. An integrated analysis of these three main components of the hydrologic cycle can provide valuable insight into the state of our understanding of the water cycle on multiple scales, as well as reveal underlying changes in the physical environment. Indeed, a subset of recent work has focused on characterizing the degree of water budget closure on regional scales. Brown and Kummerow (2014) studied the evolution of evaporation, precipitation, and divQ over five tropical ocean basins (Figure 1), finding that in most basins, closure between the components was very good despite the fully independent nature of the Evaporation, Precipitation, and divQ products. The water budget over the West Pacific, however, was shown to slowly fall out of closure in the early 2000s. While that study was not able to specifically identify why this occurred, the emergence of a lack of closure in only one of the five basins studied poses an interesting question. This trend is almost certainly not a result of satellite drift, since the same satellites provide data for all of the studied regions, and a drift would therefore be present in all five basins instead of just the West

Pacific. An initial investigation into the underlying components of the hydrologic cycle was conducted, finding that reanalyses generally produce higher magnitudes of evaporation and precipitation than observational products over the tropical oceans. Additionally, a large discrepancy between reanalysis and observational depictions of near-surface moisture was discovered, which directly impacts ocean surface evaporation magnitude (Brown and Kummerow 2014). The Brown and Kummerow study established the foundation for this work by discovering the emerging lack of closure within the Tropical West Pacific basin and the absence of a similar pattern of closure in any other region studied. This work builds upon those findings by extending the analysis further in time and attempting to determine the reason for this lack of closure. Moreover, a larger variety of products are investigated in the current work and changes in the conclusions are analyzed. The source of the emerging lack of closure is critical to investigate, as it indicates that the assumptions used in the construction of some, or all of the data products used to depict the hydrologic cycle are correct within the context of the physical

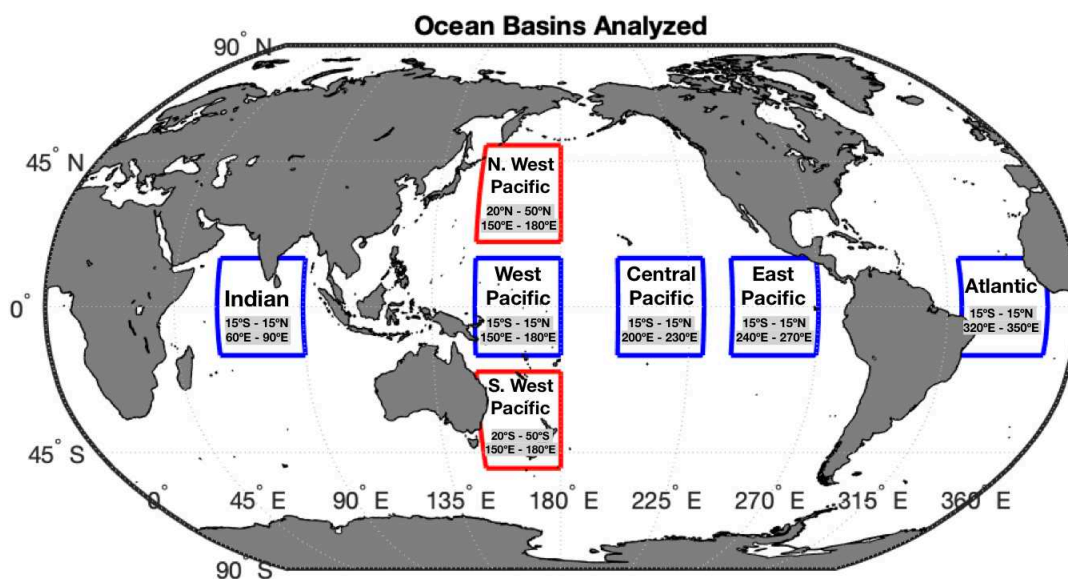


Figure 1: Ocean basins analyzed in this work. Basins also analyzed in Brown and Kummerow 2014 are outlined in blue (Adapted from Brown and Kummerow 2014).

environment in the West Pacific. Without a proper understanding of why this lack of closure is occurring, a complete understanding of the hydrologic cycle, how it relates to the global energy cycle, and how both may change in a warming climate cannot be obtained.

The goal of this work, therefore, is to identify the differences between representations of the water cycle as depicted by multiple independent products, then use the character of these differences to hypothesize the mechanisms behind the evolving lack of closure of the water cycle in the West Pacific.

CHAPTER 2: DATA AND BACKGROUND

This work relies upon multiple independent data sources to describe the state and evolution of the components of the hydrologic cycle. In general, these variables are difficult to observe directly, a challenge even more relevant at regional scales and over tropical oceans as is the focus of this work. Accurate representation of precipitation, atmospheric moisture transport ($\text{div}Q$), and latent heat flux from the ocean surface is fundamental to our understanding of the hydrologic cycle at both global and regional scales. However, continuous observational records of these quantities do not exist, and depictions of these variables are reliant on indirect satellite retrieval algorithms or on atmospheric reanalysis products. Nonetheless, in this work we aim to minimize these drawbacks by comparing the output from multiple independent datasets for each component of the hydrologic cycle. Each of the datasets utilized in this work is described in detail in the following subsections.

2.1: Evaporation

Because of the technical limitations preventing widespread in-situ measurement of ocean-atmosphere fluxes, it is necessary to calculate these fluxes using surface-level atmospheric bulk variables as input to bulk aerodynamic formulas. Specifically, the bulk formulas and parameterizations derived following the Coupled Ocean-Atmosphere Response Experiment (COARE) (Brunke et al. 2002, Fairall et al. 2003) are widely used and accepted as being among the most accurate and easy-to-apply bulk flux algorithms. These algorithms follow the convention of calculating latent heat flux as

$$LH = \rho L_v c_e U (q_0 - q_a) \quad (\text{Eq. 1})$$

Accordingly, ocean evaporation can be calculated as

$$E = \frac{LH}{\rho_w L_v} \quad (\text{Eq. 2})$$

Here, LH is the latent heat flux, E is evaporation, ρ and ρ_w are the density of air and of seawater, respectively, L_v is the latent heat of vaporization, c_e is the bulk turbulent transfer coefficient, U is the horizontal wind speed at a reference height at the surface, and q_0 and q_a are the specific humidity at the ocean surface and at a reference height above the surface, respectively.

Physically, q_0 is the saturation specific humidity at the sea surface temperature (SST). L_v (in J/kg) may be approximated as a function of SST with the empirical function

$$L_v = (2.501 - 0.00237 \times \text{SST} [^\circ\text{C}]) \times 10^6 \quad (\text{Eq. 3})$$

from Yu (2019).

Bulk aerodynamic calculations of latent heat flux require knowledge of the specific humidity at a specified level above the ocean surface, generally at either 2 m or 10 m. While satellite sensors can observe surface variables with rather high accuracy, it is difficult to directly retrieve atmospheric specific humidity and temperature at points just above the surface (Yu et al. 2008). Several techniques have been introduced to retrieve near-surface specific humidity based on values of total precipitable water and in the lowest 500 m of the boundary layer, which is more easily retrieved (Chou et al. 1995, 1997). Other methods for retrieving near-surface specific humidity utilize a more advanced approach using neural networks (Roberts et al. 2010). While the overall algorithm developed in the COARE experiment is fairly ubiquitous in observational studies and products, the method of retrieval for near-surface variables is often specifically customized to each flux product or reanalysis.

The formulas denoted above are used to calculate heat fluxes in a variety of field studies and observational gridded global flux products. Nevertheless, it is important to note that bulk

flux calculations within atmospheric reanalysis products are inherently more complex than the basic flux relations used in the COARE algorithm. By definition, an atmospheric reanalysis assimilates observational data to constrain predictions from an underlying numerical model to allow the reanalysis to output variables on a standard global grid, regardless of the location of the assimilated observations (Roberts et al. 2011). However, the application of bulk parameterizations in each reanalysis differs depending on how the underlying model handles relevant aspects such as the relationship between ocean surface characteristics and bulk turbulent transfer. As such, the values of parameters such as heat flux or evaporation can vary widely between reanalysis products due to different parameterizations of the exchange coefficient within the underlying model (Roberts et al. 2011). Within the observational flux products analyzed in this work, the exchange coefficient and thus the latent heat flux are parameterized and calculated according to the conventions set forth in COARE version 3.0 (Fairall et al. 2002). In contrast, within the reanalysis products, the parameterizations and conventions are generally more opaque to the user.

Within this work, we evaluate the differences between the evaporation and flux output from one observational ocean flux dataset, one pseudo-observational flux dataset, and two atmospheric reanalyses. SeaFlux (Curry et al. 2004, Clayson et al. 2013) is a global dataset consisting of surface heat fluxes over the ice-free oceans and the satellite-derived bulk atmospheric variables used to calculate these fluxes. OAFlux (Yu and Weller 2007, Yu et al. 2008) is a global dataset consisting of essentially the same products as the SeaFlux dataset. However, while all SeaFlux output is derived from observational satellite data, OAFlux is fundamentally different in its construction in that it combines satellite data with reanalysis data as part of an objective analysis approach designed to reduce the overall error of the bulk

variables. As a result, OAFlux is considered a pseudo-observational dataset, while SeaFlux is purely observational. For simplicity, SeaFlux and OAFlux will hereafter be collectively referred to as “observationally-based flux products”. ERA-5 (Hersbach and Dee 2017, Hersbach et al. 2019) is produced by the European Centre for Medium-Range Weather Forecasts (ECMWF) and is a next-generation reanalysis intended to replace ERA-Interim (Dee et al. 2011). NASA’s Modern-Era Retrospective Analysis for Research and Applications, Version 2 (MERRA-2) is an update to the original version of MERRA (Reinecker et al. 2011) intended to improve upon known deficiencies in MERRA, upgrade the underlying model, and incorporate the assimilation of new observational data types (Gelaro et al. 2017). Because SeaFlux, OAFlux, ERA-5, and MERRA-2 are a diverse representation of the current state-of-the-art, they will be the four products used for the depiction of ocean surface evaporation in this study. Monthly average evaporation in each tropical ocean basin from 1998 to 2016 is plotted in Figure 2 for SeaFlux, ERA-5, and MERRA-2. Within Figure 2, it is obvious that both ERA-5 and MERRA-2 exhibit distinctly larger magnitudes of ocean surface evaporation than SeaFlux over all basins. There is a seasonality to these differences, as both reanalysis products exhibit a more pronounced seasonality in evaporation magnitudes than SeaFlux. Also notable is a slight warming trend in SSTs over the period of study that is not seen in the evaporation data of any of the products as these evaporation products respond more closely to the near surface wind speed and moisture deficit.

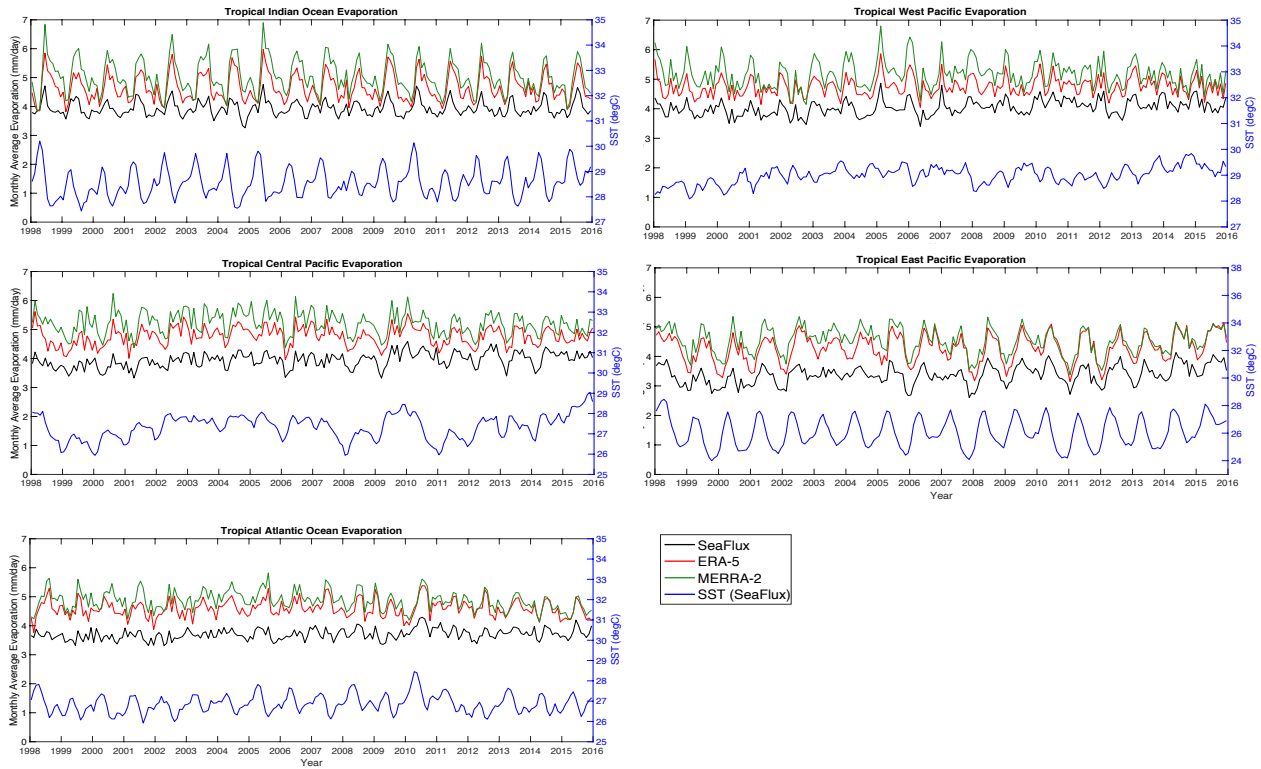


Figure 2: Monthly average evaporation over all tropical ocean basins for SeaFlux, ERA-5, and MERRA-2.

SeaFlux output is entirely based on satellite observations. SSTs are sourced from the Optimally-Interpolated Version 2.0 SST dataset which is based on infrared observations from the Advanced Very High Resolution Radiometer (AVHRR) (Reynolds et al. 2007). Wind speed is based on the Cross-Calibrated Multi-Platform (CCMP) Ocean Surface wind dataset. Near-surface specific humidity values are sourced from the Special Sensor Microwave/Imager (SSM/I). Since these near-surface values cannot accurately be observed directly due to technical limitations, a neural network approach is utilized to retrieve these values in addition to supplemental wind speed data. This method is explained briefly in this section and is described in greater detail in Roberts et al. (2010). Past retrieval methods for near-surface moisture from microwave satellite observations were based on linear regression between near-surface properties and microwave satellite observations, despite these relationships often being distinctly non-

linear. To adapt to the nonlinearity of this relationship, Roberts et al. (2010) introduce a neural network designed to retrieve near-surface humidity, among other variables, using microwave radiances as input. This new method is noted to produce values of near-surface specific humidity that have the lowest root-mean-square error of all other tested methods. This gives SeaFlux an advantage over other flux datasets, in that SeaFlux uses values of near-surface specific humidity from the Roberts et al. (2010) neural network as input to the COARE bulk flux algorithm rather than values from numerical models. However, one must still recognize the disadvantages of the neural network approach used in SeaFlux. As with any other neural network, the quality of the data used to train the network greatly affects how well the retrieval performs with certain inputs. The Roberts et al. (2010) neural network is noted to be relatively inaccurate in cases of high wind speeds and high cloud liquid water content. Nevertheless, the use of this neural network approach allows SeaFlux to utilize relatively high-accuracy data as input to the COARE bulk algorithm and remain a purely satellite-based observational dataset.

OAFflux is significantly different than SeaFlux in that it is a blended dataset that uses an objective analysis approach to combine the distinct advantages of both satellite and atmospheric reanalysis data to select input bulk variables for the COARE algorithm that have the greatest accuracy (Yu and Weller 2007, Yu et al. 2008). Satellite data sources for OAFflux are similar to those for SeaFlux, but OAFflux also sources data from the NCEP1, NCEP2, and ERA-40 reanalyses. These data are synthesized in a way that seeks the minimum variance between analysis values and truth values. This is accomplished by assigning a weight to each satellite and reanalysis input source based on the error covariance of the sources, which is obtained from climatology and in situ buoy measurements. In a distinct contrast to SeaFlux, OAFflux does not obtain input bulk variable data from a single source type. This gives OAFflux a unique set of

strengths and weaknesses. On one hand, the objective analysis approach allows for high confidence in a certain degree of accuracy among the variables, since each input source is weighted according to the climatological fit to various direct measurements. On the other hand, the lack of total independence between OAFlex and reanalysis products must also be considered when utilizing OAFlex output.

As described previously, atmospheric reanalysis products are useful for climate-scale studies due to their ability to present continuous, uniformly gridded data in both the spatial and temporal dimensions. This is especially true for evaporation due to the difficulty in obtaining direct observations. Despite the utility of reanalysis depictions of ocean evaporation, care must be taken when using these data due to the opacity of the assumptions made in the construction of the reanalysis. Whereas the data used in observational products such as SeaFlux is well-documented and generally stationary, this is generally not the case with reanalysis products, as observations change over time and the underlying model within the reanalysis may exhibit biases that are not well-documented.

2.2: Precipitation

In general, precipitation is very difficult to directly measure, as it is highly variable in both space and time. Individual precipitation features can exhibit a large range of possible magnitudes and spatial scales. Direct measurement of precipitation is a challenging task made even more difficult over oceans where surface-based sensors are impractical to continuously implement and are limited to ships or islands. As a result, satellite-based sensors have been and likely will continue to be the platform of choice for precipitation observations for the foreseeable future. It is important to note that precipitation is indirectly measured, and magnitude of rainfall is determined using ever-evolving retrieval algorithms using a variety of spaceborne sensors.

Central to the improvement of modern precipitation retrievals has been the advances in remote sensing of precipitation made during the Tropical Rainfall Measurement Mission (TRMM) (Kummerow et al. 1998) from 1998 to 2015 and successor Global Precipitation Measurement (GPM) mission (Hou et al. 2014), launched in 2014. Both the TRMM and GPM missions carried an active precipitation radar aboard the main spacecraft. In the case of TRMM, this was the first precipitation radar flown in space, and it and the successor instrument aboard GPM were able to provide detailed three-dimensional characterization of precipitating clouds. While this is the most direct method of measurement available, radar measurements are very infrequent and therefore are challenging to implement into a large-scale continuous product. Also flown during both TRMM and GPM was a passive microwave radiometer. In contrast to the precipitation radar, the radiometer is a passive instrument which observes the microwave signature emitted by both the surface and precipitating clouds. Consequently, passive microwave observations are less direct than radar observations, but hold an advantage in that much higher sampling area is available due to a larger swath and the scanning nature of the instrument. Both radar and radiometer observations are currently limited to low-Earth orbiting satellites, which inherently are limited in temporal sampling coverage. In contrast, geostationary satellites provide continuous temporal coverage and can continuously observe a much larger area than low-Earth orbiting sensors. However, because of the very large physical distance between a geostationary satellite and the earth, the types of observations are generally limited to conventional visible and infrared bands. Algorithms which relate visible and infrared radiances to rain rate do exist and have the advantage of having the largest sampling capabilities, but these are generally the most ambiguous and least direct methods for observing precipitation.

While the individual radar and radiometer observations are valuable, both methods depend on retrieval algorithms to convert raw observed radiances into interpretable precipitation metrics. Within this work, we compare the output of two popular gridded precipitation datasets, the Global Precipitation Climatology Project (GPCP) and the Integrated Multi-Satellite Retrievals for GPM (IMERG). It should be noted that these two products differ fundamentally in their respective goals. GPCP is constructed with temporal consistency as a top priority and is intended to avoid the inconsistencies associated with sensor changes, thus serving a role as a climate data product for precipitation. In contrast, IMERG was constructed with a goal of providing the best possible estimate of precipitation at a given time using as many sensors and data sources as possible. Consequently, IMERG is more prone to inhomogeneities associated with the addition or removal of sensors from orbit, and is prone to errors resulting from the merging algorithm itself. Despite the differences between the two products, both GPCP and IMERG provide gridded high-resolution estimates of global precipitation which are continuous in time. The basic theory and operation of each of these products is described here, and more detailed information can be found in the cited literature.

The GPCP precipitation product has an extensive legacy dating back to 1997 with the debut of Version 1. As mentioned previously, GPCP is intended to provide a stable, long term analysis of precipitation which is free of the biases and errors associated with sensor changes. The Version 2 product analyzed here provides a monthly estimate of precipitation at 2.5-degree grid resolution. A related higher resolution product is also analyzed, characterizing precipitation at daily temporal and 1-degree grid resolution. As GPCP is a merged dataset, it utilizes multiple separate precipitation products as inputs to create the final gridded analysis value, which is a best estimate created by combining various aspects of the input datasets. Most prolific of the input

data are microwave radiances observed by the Special Sensor Microwave Imager (SSM/I) and its later iterations from 1987 onward. These data comprise the foundation of the GPCP dataset, with precipitation estimates retrieved over ocean from the 19- and 22-GHz channels using a histogram-based retrieval (Wilheit et al. 1990). A scattering-based algorithm utilizing the 85-GHz channel retrieves precipitation over land. Due to the spatial and temporal limitations of microwave observations resulting from their reliance on polar orbiting satellite systems, other data sources must be used to fill in temporal gaps. With their continuous spatial and temporal coverage, geostationary observations are well-suited to this purpose. However, observations useful for retrieving precipitation are limited to the infrared bands, which can only observe cloud-top characteristics and cannot provide insight regarding in-cloud precipitation structure. Nevertheless, these geostationary infrared observations can be related to precipitation using retrievals which correlate cold cloud top area with rain rate. In addition to geostationary infrared observations, retrieved atmospheric characteristics from polar orbiting infrared sounders are used to infer precipitation in areas where SSM/I microwave data are unavailable or unreliable. GPCP also utilizes a collection of gridded rain gauge data from the Global Precipitation Climatology Centre (GPCC). In the creation of the final precipitation estimate product, GPCP joins the precipitation estimates from each respective product into a monthly composite. These satellite-based estimates are then blended with gauge data where it is available, mostly over land. Consequently, GPCP estimates of precipitation over oceans are mostly satellite-based, as there are few rain gauges located outside of continental land masses.

In general, GPCP achieves its goal of maintaining a stable climate data record of precipitation over time through a relatively small range of input datasets. Most notable in this approach is that the passive microwave observations are entirely sourced from the SSM/I family

of sensors. While this allows for a temporally stable data record, in modern times there is an increasing number of other satellite platforms capable of delivering passive microwave observations for precipitation estimation. In contrast to GPCP, IMERG seeks to create the highest resolution, most accurate estimation of global precipitation at any given time. This requires the use of multiple different satellites and input data which results in a reduction of temporal homogeneity compared to GPCP.

IMERG relies on many similar input datasets as GPCP but is notably different in its use of passive microwave observations. Of central importance in IMERG is the role of the Global Precipitation Measurement Core Observatory (GPM-CO) satellite, launched in 2014 as a successor to TRMM. IMERG is unique in that it relies on data from as many “satellites of opportunity” as are available. That is, instead of relying on a single sensor type, IMERG is flexible in that it is able to utilize passive microwave observations from any microwave radiometer with available data. Precipitation is estimated from these observations using GPROF (Kummerow et al. 2015), and all data is calibrated to estimates from the GPM-CO. Within this framework, IMERG is not limited to a single input source of passive microwave precipitation estimates. Despite the large amount of passive microwave data available to IMERG, continuous global coverage is still not achieved with passive microwave observations alone. To combat this, IMERG employs a morphing scheme to fill in the temporal gaps of the microwave observations. This scheme, based on the CMORPH algorithm (Joyce et al. 2011), uses geostationary infrared observations to compute propagation vectors which allow for temporal interpolation of precipitation features between successive passive microwave observations. Precipitation estimates are also supplemented with microwave-calibrated infrared estimates obtained using the PERSIANN-CCS algorithm (Hong et al. 2004). Within the PERSIANN-CCS algorithm, a neural

network approach is used to estimate precipitation based on the characteristics of infrared-observed cloud properties. In a similar fashion as GPCP, IMERG also utilizes GPCC gauge estimates of precipitation within the merging procedure and for calibration purposes.

The backbone of the IMERG algorithm are estimates of precipitation from GPROF (Kummerow et al. 2015). While GPROF is proven and is quite versatile in its applicability to different sensors and situations, it is not without drawbacks which affect its accuracy. Recent work has analyzed the effect of dominant convective type and level of organization on the accuracy of precipitation retrieved from the TRMM Microwave Imager (TMI) using GPROF. This work has found that GPROF generally underestimates rain rates in cases of isolated deep convection by as much as 37.8%. In contrast, GPROF overestimates rain rates where precipitation is characterized by organized deep convection by as much as 33.4% (Henderson et al. 2017). Cases of deep isolated convection in this context are characterized by relatively small deep convective cores, while cases of deep organized convection are characterized by a large amount of deep stratiform rain in addition to deep convective cores. When isolated convection is the dominant mode, the small areal extent of the convective core with respect to the relatively large footprint of the TMI can result in significant underestimation of the rain rate. When organized convection is the dominant mode, the very large fraction of stratiform rain present within the anvil clouds of organized systems results in an overestimation of rain rate by GPROF. This is generally due to difficulties within GPROF in resolving the differences between convective and stratiform precipitation related to the fraction of convection within the TMI field of view (Carr et al. 2015, Henderson et al. 2017). Because the biases appear to be related to inhomogeneities in the field of view, it is likely that these errors exist for other algorithms (e.g. Wilheit et al., 1990) as well, although specific work has not been done with other algorithms or

products. The differing behavior of GPROF, potentially in addition to other algorithms, in different environmental situations is important to consider when studying temporal patterns of precipitation, especially in regions where dominant convective mode can vary significantly. By this logic, large trends in precipitation magnitude or changes in the relationship between different products may be an algorithm artifact rather than an actual change in the magnitude of precipitation. This, as well as all algorithm nuances, is crucial to consider when analyzing long-term patterns of precipitation.

Figure 3 displays the smoothed monthly average raw precipitation rates for all products over all basins. An initial analysis of Figure 3 reveals that the relationship between the depictions of the individual products varies by basin. In a similar manner to the evaporation comparison, reanalysis depictions of precipitation seem to exceed the observational depictions in terms of magnitude. Much work has focused on the bias between observations and modeled depictions of precipitation over the oceans (e.g. Austin et al. 1995, Stephens et al. 2010, Ahlgrimm and Forbes 2013), often finding an excess production of drizzle within models. In addition, seasonality in precipitation magnitude seems most pronounced in the Indian Ocean, East Pacific, and Atlantic Ocean basins, whereas the West and Central Pacific basins appear to exhibit lower-frequency variability. The implications and plausible reasons behind this are examined in detail in a later section.

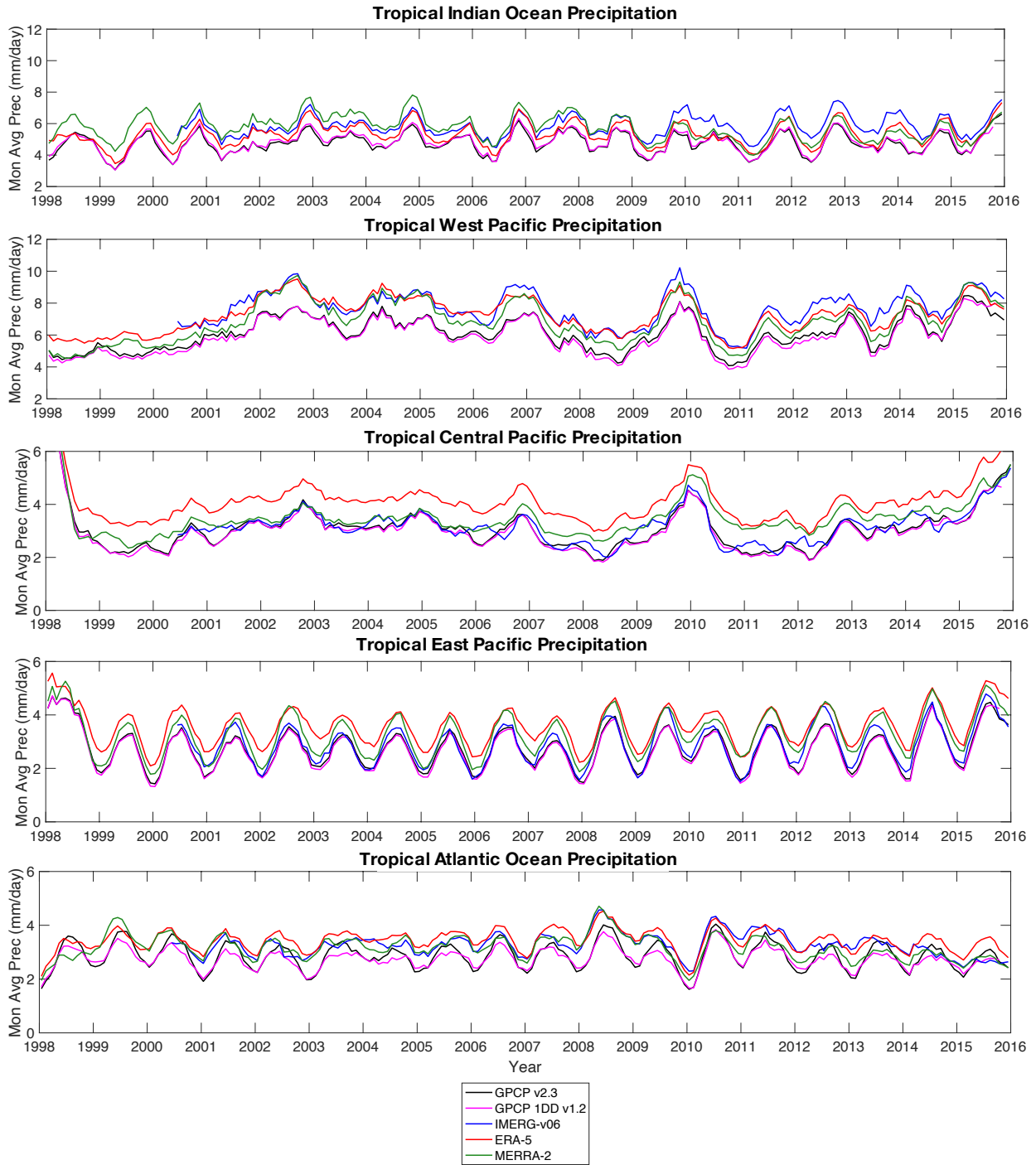


Figure 3: Monthly average precipitation rates over all tropical ocean basins for GPCP v2.3, GPCP 1DD, IEMRG v6, ERA-5, and MERRA-2.

2.3: Atmospheric Water Vapor Flux Divergence

The general atmospheric water budget (Peixoto and Oort 1992) over the oceans can be expressed in the form:

$$\frac{\partial W}{\partial t} + \nabla \cdot \frac{1}{g} \int_0^{p_0} (q\vec{V}) dp = (E - P) \quad (\text{Eq. 4})$$

The first term on the left-hand side of this equation is the water vapor tendency term, and the second term on the left-hand side of the equation is the vertically integrated water vapor flux divergence (hereafter referred to as divQ). The right-hand side of the equation represents freshwater flux, which is the difference between magnitudes of ocean evaporation and precipitation. The tendency term can be assumed to be zero at large temporal scales; therefore, the water budget over the oceans simplifies to the balance between divQ and the freshwater flux.

As discussed previously, there are methods for observing both evaporation and precipitation over oceans, although these methods are imperfect and susceptible to errors. Without vertically resolved wind observations, it is difficult to observe the quantity divQ on any scale, and retrieval methods that use proxy variables (e.g. Hilburn 2009, Xie et al. 2008) are still relatively new and untested. Therefore, quantities of divQ used in this and other studies are generally extracted from atmospheric reanalysis datasets. While reanalysis data has the advantage of being gridded, continuous, and high resolution, this data should also not be assumed to be perfect, due to the ambiguity introduced by the assimilation scheme, observational network, and underlying numerical model used in the production of the reanalysis. A very brief descriptions of the reanalysis datasets used in this study are included here, but the reader is encouraged to review the cited literature for a more detailed overview of each reanalysis framework. A time series comparison of ERA-5, ERA-Interim, and MERRA-2 depictions of divQ for the West Pacific is shown in Figure 4. This exemplifies the varying relationship

between the depictions of each reanalysis products over time, and will be discussed in detail in a future section.

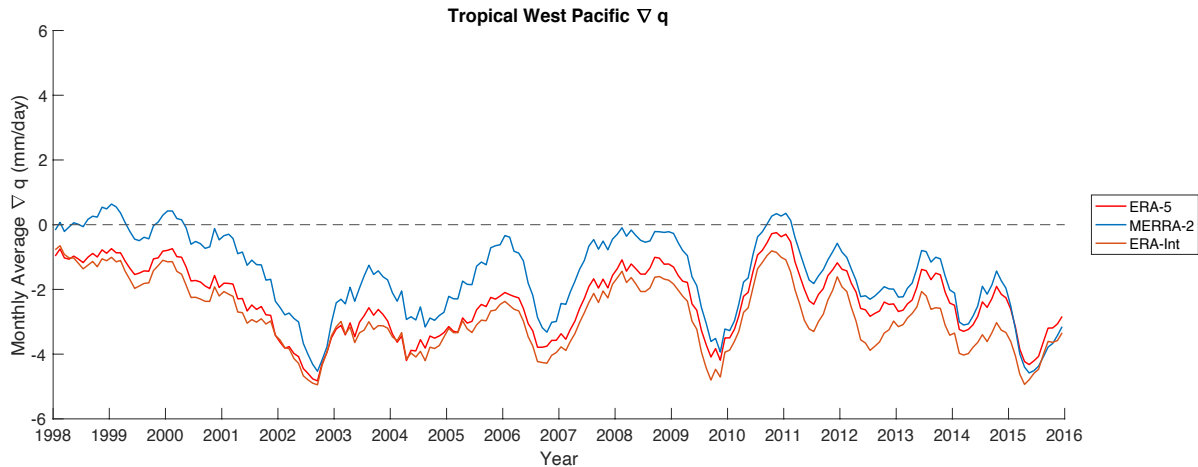


Figure 4: Smoothed time series comparison of ERA-5, ERA-Interim, and MERRA-2 depictions of $\text{div}Q$ for the West Pacific basin.

The Modern-Era Retrospective Analysis for Research and Applications, Version 2 (MERRA-2) is the current reanalysis produced by the National Aeronautics and Space Administration (NASA). The underlying numerical model within MERRA-2 is the Goddard Earth Observing System (GEOS). MERRA-2 is a notable improvement upon its predecessor due to the reduction of spurious trends in water cycle components, and is more resilient to observing system changes (Gelaro et al. 2017). The other reanalysis datasets used in this study are produced by the European Centre for Medium Range Weather Forecasts (ECMWF). The older of these is the ECMWF Reanalysis – Interim (ERA-Interim) (Dee et al. 2011), and the current state-of-the-art from ECMWF is the ERA-5 reanalysis (Hersbach et al. 2020). Both versions of ERA studied here utilize the Integrated Forecast System (IFS) as the data assimilation system. The main differences between ERA-Interim and ERA-5 mainly relate to the underlying model, the

addition of new observational datasets, and the resolution of the output. All three of the reanalysis products mentioned here output quantities needed to compute $\text{div}Q$ within this work.

CHAPTER 3: RESULTS AND ANALYSIS

The primary goal of this work is to better understand the temporal evolution and stability of the products commonly used to represent the individual components of the atmospheric branch of the hydrological cycle. With the resulting insight on how independent products relate to one another and how these relationships evolve with time, we can obtain an understanding of how each product, and thus each component, relates to the evolution of the water cycle. Since each product analyzed as part of this work is produced at differing native resolutions, all data was aggregated into monthly averages and analyzed at a common 1-degree grid scale. The reasons for this are twofold. First, despite the fact that much of the data (e.g. reanalysis data) is available at finer resolution, it is advantageous to maintain an analysis at 1-degree resolution for continuity with prior work. Second, a monthly average temporal scale was determined to be adequate for this analysis because of the focus on trends observed in the water cycle and consistency among products rather than process understanding, which requires higher temporal resolution.

In this section, a common analysis framework is applied to each component of the atmospheric hydrologic cycle and closure as a whole, and the results discussed. For each ocean basin, each of the products discussed in the preceding section are compared to one another in qualitative and quantitative fashions at multiple scales. Then, differences between products are noted and the reasons behind these differences are hypothesized. To conclude the analysis, the effects of individual component trends or product differences are related back to the evolution and magnitude of overall hydrologic cycle closure.

3.1: Evaporation

Figure 5 shows the zonal average of latent heat flux and evaporation for both June and December 2007. From this figure, it is clear that on a global scale, latent heat flux and evaporation magnitudes in both reanalyses exceed those in both SeaFlux and OAFlux, in some cases by as much as 50 W/m^2 or approximately 2 mm/day . The largest differences are found within tropical subsidence regions. Within these tropical subsidence regions, MERRA-2 produces the highest values of latent heat flux and evaporation, with ERA-5 producing slightly

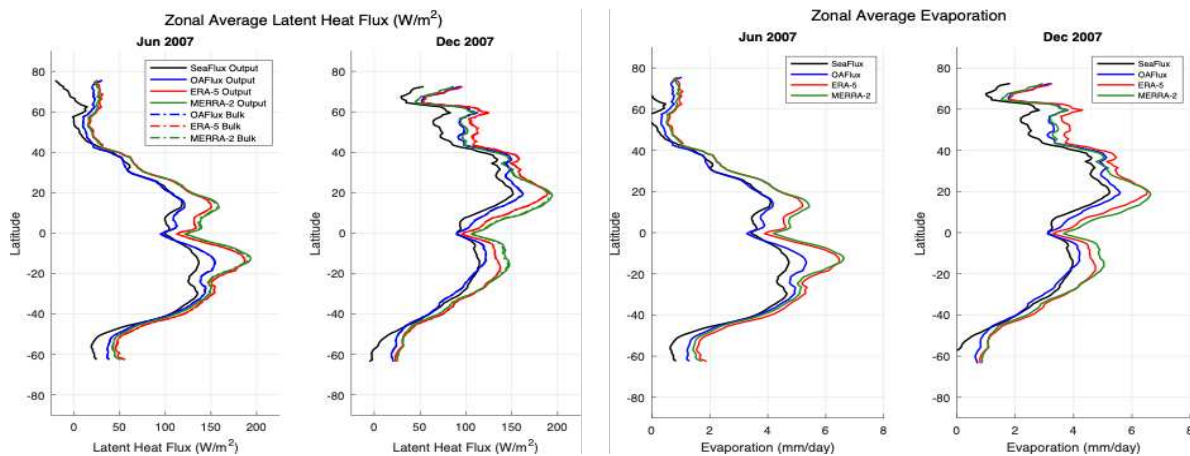


Figure 5: Global zonal averages of latent heat flux and evaporation for June and December 2007

smaller values. At these low latitudes, MERRA-2 evaporation is about 31% larger in June and about 26% larger in December than an aggregate of the two observationally-based flux products while ERA-5 evaporation is about 26% larger in June and about 17% larger in December than the two observationally-based flux products. The two reanalyses generally exhibit similar characteristics with respect to one another in terms of flux magnitude, and when considered together behave distinctly differently than the two observationally-based flux products. Both SeaFlux and OAFlux also seem to behave in a similar manner to one another and can roughly be conceptualized as one pair in comparison with the reanalysis pair. Overall, within tropical

latitudes, SeaFlux produces the lowest values of latent heat flux and evaporation, with OAFlux producing slightly higher values. This pattern of the two reanalyses producing notably higher flux values than the two observationally-based flux products is most robust in the tropical subsidence regions.

Within the tropics, reanalyses systematically produce distinctly higher flux magnitudes than observationally-based products. This pattern can be seen in Figure 6, which compares latent heat flux and evaporation between products within the Central Pacific Ocean basin.

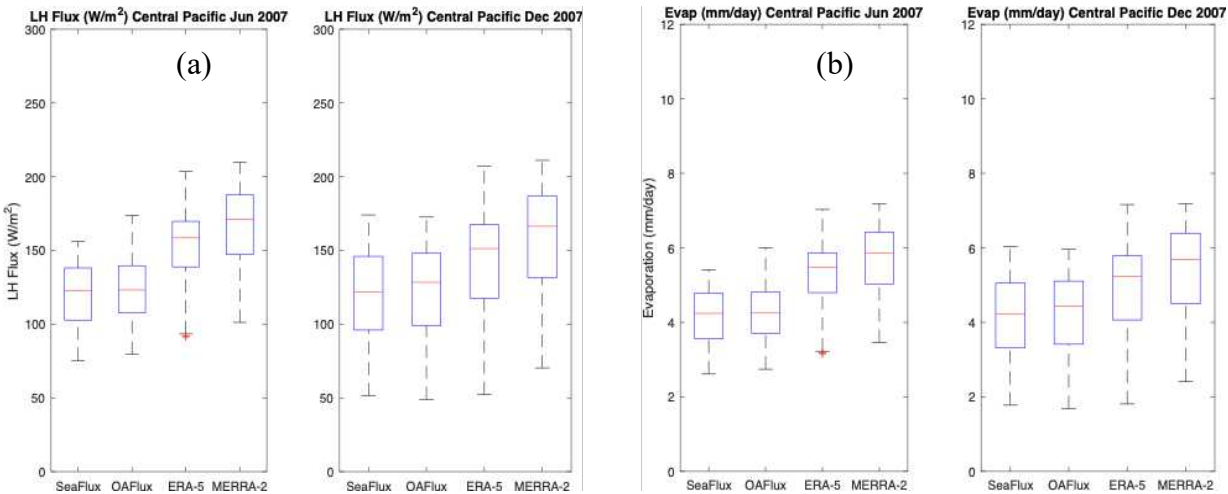


Figure 6: (a) Latent heat flux and (b) evaporation for all products within the Central Pacific tropical ocean basin (-15 to 15 degrees latitude, 200 to 230 degrees longitude)

The remaining four tropical ocean basins (not shown) generally exhibit a similar pattern to the Central Pacific. At higher latitudes, this pattern is also present, but the magnitude of difference between the reanalyses and the observationally-based flux products is greatly reduced relative to the difference at tropical latitudes. In addition, at higher latitudes ERA-5 produces the largest values of latent heat flux and evaporation, whereas MERRA-2 produces the largest values in the tropics. At latitudes greater than 15 degrees, ERA-5 evaporation is about 22% higher in June and about 23% higher in December than the observationally-based flux product evaporation.

MERRA-2 is about 17% and 20% higher than the observationally-based products in June and December, respectively.

The notable differences between products, as well as in relative flux magnitudes between tropical and higher latitudes, invite an exploration into the characteristics of the underlying bulk variables that are used to calculate the magnitudes of these fluxes. In this way, we can better understand the evaporation output from each product within the context of how each product was created. SeaFlux and OAFlux use an adapted version of the COARE algorithm to calculate latent heat flux. Within atmospheric reanalyses, differing assimilation schemes and parameterizations result in a less tractable picture of how latent heat flux and evaporation are calculated. Nevertheless, the same bulk variables used in the COARE algorithm are useful in understanding the algorithms used to compute fluxes in reanalyses. Accordingly, we analyze SST, near-surface wind speed (U), ocean surface specific humidity (q_0), and near-surface specific humidity (q_a) in an attempt to gain insight into the characteristics of the various products and why patterns in flux output differ between tropical and high latitudes. In SeaFlux, ERA-5, and MERRA-2, the atmospheric reference level representing “near-surface” is 10 meters above the ocean surface, whereas in OAFlux, this value is taken as 2 meters above the ocean surface.

Of the bulk variables analyzed here, SST is the most spatially uniform and the most consistent variable among the different products on a monthly average temporal scale. Globally, reanalysis and observational SST magnitudes exhibit differences of negligible magnitude. However, it should be noted that slightly higher differences exist in boundary current regions where temporal variability of SST is greater than other regions. Since ocean surface specific humidity (q_0) is proportional to the sea surface temperature through Equation 3, q_0 exhibits

essentially the same global-scale variability as SST, indicating the close coupling between these two quantities.

By Equation 1, the quantity $(q_0 - q_a)$, which represents the near-surface moisture gradient, is proportional to the latent heat flux. Figure 7 presents global zonal average values of q_0 , q_a , and $(q_0 - q_a)$. From Figure 7a, it is clear that q_0 is consistent between products. Zonal average SSTs (not shown) exhibit a nearly identical pattern, which is justified since the two quantities are directly related. In contrast, as seen in Figure 7b, both reanalyses produce values of q_a that are quite low relative to the observationally-based flux products.

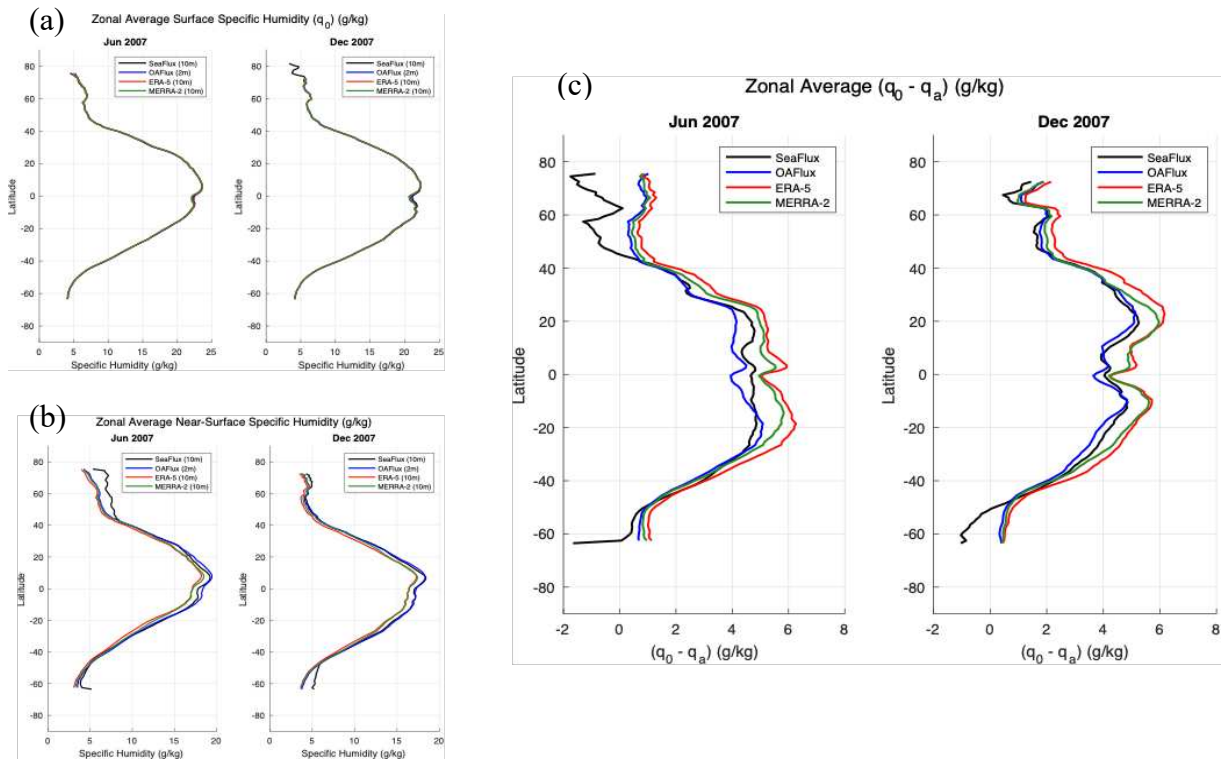


Figure 7: (a) Zonal average ocean surface specific humidity, (b) zonal average atmospheric near-surface specific humidity, and (c) zonal average $(q_0 - q_a)$.

This relationship is most robust in the tropical latitudes, where ERA-5 and MERRA-2 each produce slightly more than 5% lower q_a values than the observationally-based flux products.

This pattern can be seen more closely in Figure 8b, which illustrates the same patterns within the

tropical Central Pacific basin. Here, we can also see that while q_0 remains fairly uniform across products, q_a in both reanalyses is distinctly lower than in both observationally-based flux products.

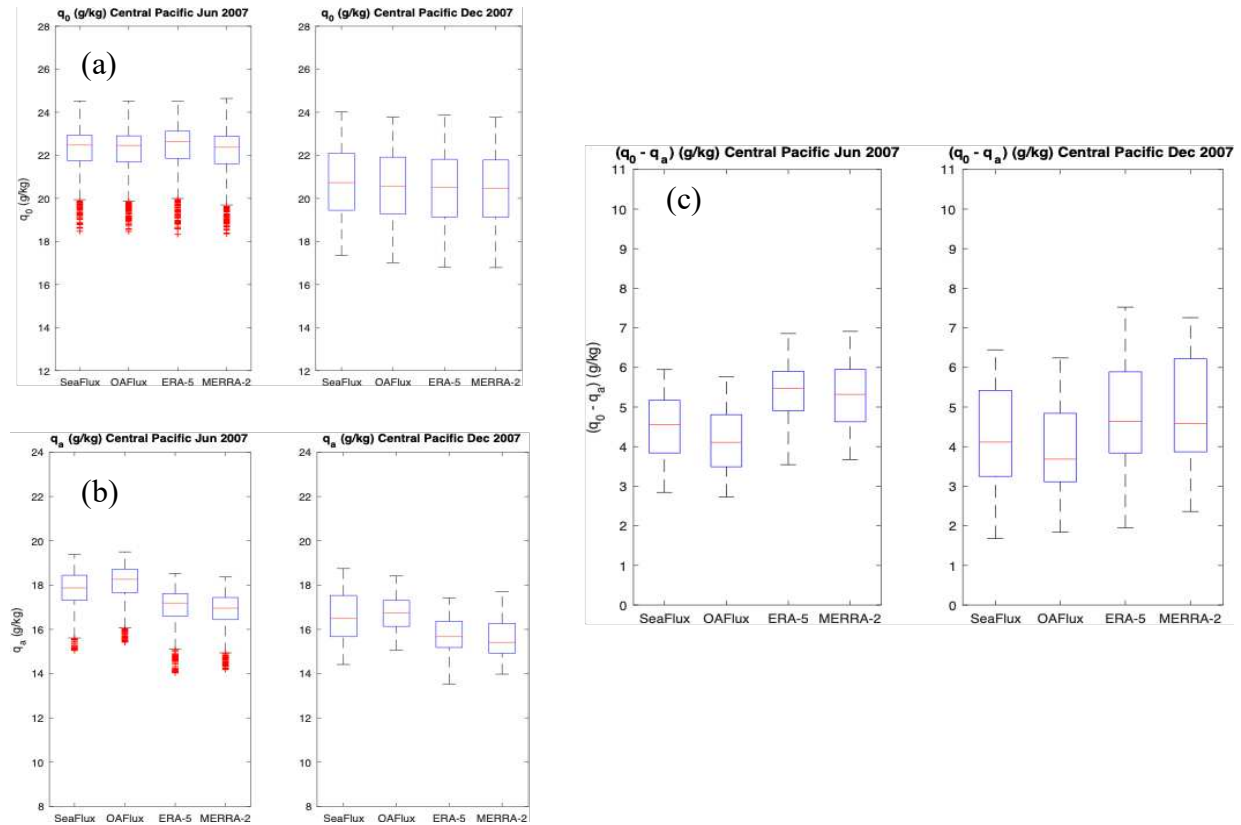


Figure 8: (a) Central Pacific ocean surface specific humidity, (b) Central Pacific atmospheric near-surface specific humidity, and (c) Central Pacific ($q_0 - q_a$).

At higher latitudes outside the tropics, this pattern is less robust. As seen in Figure 7b, reanalysis values of q_a at high latitudes are still smaller than those in flux products, but the difference is far less dramatic. Also evident in Figure 7b is very large values of q_a within SeaFlux relative to the other products at high latitudes. Higher values of ($q_0 - q_a$) imply that a drier near-surface atmosphere is present and a larger latent heat flux would consequently be expected. In Figure 7c, values of ($q_0 - q_a$) in both reanalyses are clearly larger than in the observationally-based flux products. This is especially true in the tropics, but also seems to be the case at high latitudes.

Similar to $(q_0 - q_a)$, within Equation 2 near-surface wind speed is also directly proportional to the magnitude of latent heat flux and evaporation. Figure 9 shows the global zonal average wind speed at 10 meters above the ocean surface for all four products. Immediately evident in Figure 9 is relatively good agreement between products at tropical latitudes contrasting with very poor agreement at high latitudes. At latitudes less than 15 degrees,

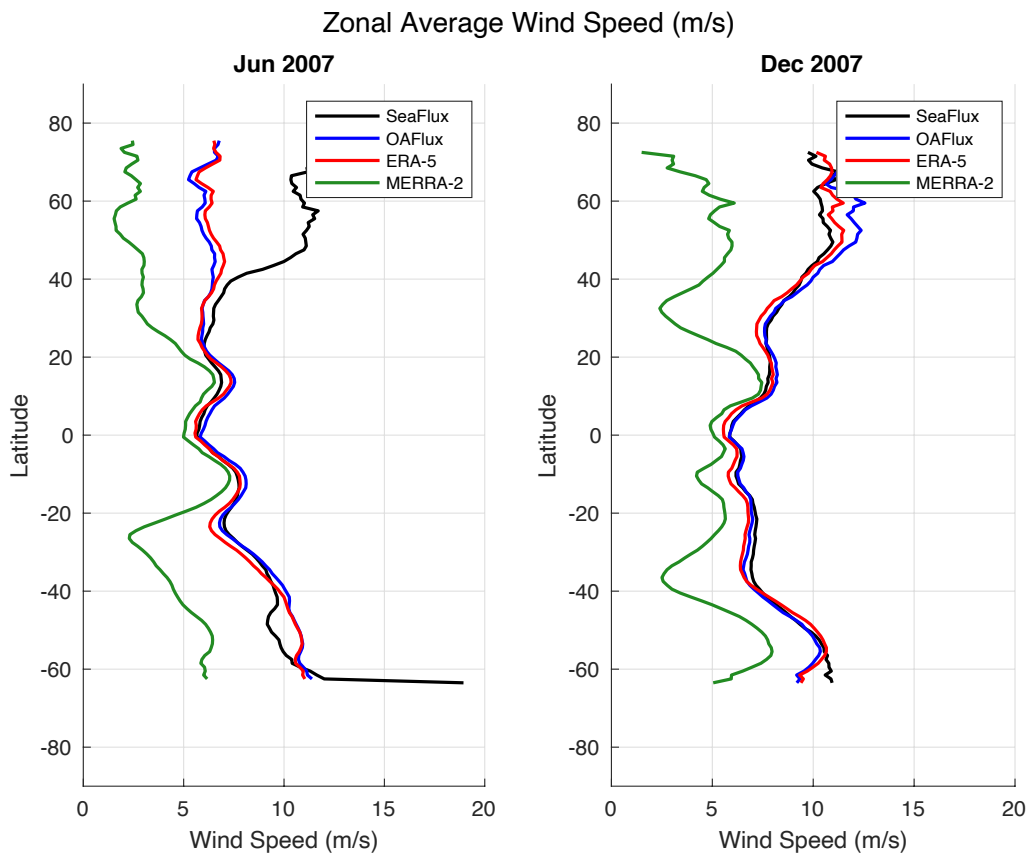


Figure 9: Global zonal average near-surface wind speed for June and December 2007.

ERA-5 wind speeds are about 2% smaller in June and about 4% smaller in December than averaged flux product wind speeds. MERRA-2 wind speeds are about 11% smaller in June and about 17% smaller in December than averaged observationally-based flux product wind speeds. At latitudes greater than 15 degrees, MERRA-2 wind speeds are about 39% smaller in December than averaged observationally-based flux product wind speeds, while ERA-5 wind speeds are

only about 1% smaller. ERA-5 wind speeds in June are only about 2% smaller than OAFlux speeds, while MERRA-2 wind speeds are about 48% smaller than OAFlux speeds.

A crucial component to any algorithm relating bulk variables to latent heat flux is the bulk turbulent transfer coefficient for latent heating, denoted in Equation 1 as c_e . This coefficient is constructed based on processes important to ocean-atmosphere interaction such as surface roughness, wave characteristics, and wind (Yu 2019, others cited therein). Understanding how c_e varies among products and between regions will provide additional insight for characterizing the depiction of evaporation within each product. However, the value of c_e is not a direct output of any of the products analyzed. To study the characteristics of the transfer coefficient, Brown and Kummerow (2014) modified the general bulk formula (Equation 1) to allow for the calculation of an Effective Transfer Coefficient (ETC) value for each product using their respective bulk variables as $ETC = \frac{E}{\rho U (q_0 - q_a)}$. Brown and Kummerow (2014) found that the ETC among the reanalysis products ERA-Interim and MERRA is generally larger than the ETC of SeaFlux throughout the tropical ocean basins studied.

Figure 10 compares the average latent heat flux, wind speed, and near-surface moisture gradient within each ocean basin for each product studied for the month of June in 2007. From Figure 10a, it is clear that during this subset of time, all tropical ocean basins follow a similar pattern, where SeaFlux produces the smallest magnitudes of latent heat flux, followed by OAFlux, then ERA-5, with MERRA-2 producing the largest magnitudes. In the midlatitude West Pacific basins, SeaFlux still produces the smallest magnitudes of latent heat flux, but ERA-5 and MERRA-2 are closer to each other in magnitude. Overall across all seven basins, OAFlux latent heat fluxes are 7.3% larger, ERA-5 fluxes are 27.7% larger, and MERRA-2 fluxes are 33.5% larger than latent heat fluxes in SeaFlux. In Figure 10b, we see that in the tropical Indian, West

Pacific, and Atlantic basins, near-surface wind speed is in relatively good agreement among products. This contrasts with the East Pacific, Northern and Southern West Pacific, and the Central Pacific, where MERRA-2 wind speeds are significantly lower than the other products. However, in these same basins with the exception of the Northern West Pacific, the wind speeds among SeaFlux, OAFlux, and ERA-5 are similar to each other and are much larger than in

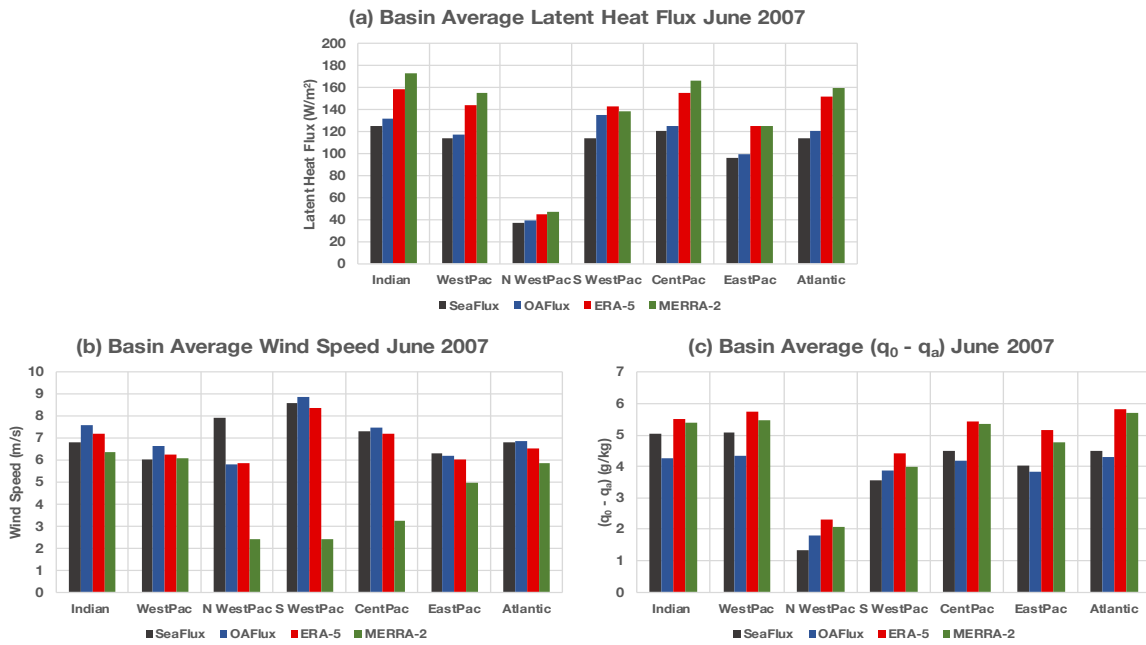


Figure 10: (a) Average latent heat flux, (b) average wind speed, and (c) average near-surface moisture gradient in all products and all basins.

MERRA-2. Across all seven basins, wind speeds in OAFlux are 0.1% lower, wind speeds in ERA-5 are 4.1% lower, and wind speeds in MERRA-2 are 34.1% lower than wind speeds in SeaFlux. Figure 10c shows the near-surface moisture gradient, calculated as $(q_0 - q_a)$, for all products and all basins. Here, it is clear that both reanalysis products produce very similar values of $(q_0 - q_a)$ in all basins, and the values of $(q_0 - q_a)$ in both ERA-5 and MERRA-2 are always larger than the values of $(q_0 - q_a)$ in SeaFlux and OAFlux. In all basins except the Northern and Southern West Pacific where the opposite is true, OAFlux produces slightly lower values of

$(q_0 - q_a)$ than SeaFlux; however, both SeaFlux and OAFlux $(q_0 - q_a)$ values are smaller than both reanalyses. This implies that the reanalyses maintain a near-surface atmosphere that is drier than in SeaFlux and OAFlux, resulting in higher magnitudes of $(q_0 - q_a)$ in ERA-5 and MERRA-2 in all basins. Across all seven basins, $(q_0 - q_a)$ in OAFlux is 0.2% lower, $(q_0 - q_a)$ in ERA-5 is 28.2% higher, and $(q_0 - q_a)$ in MERRA-2 is 20.8% higher than $(q_0 - q_a)$ in SeaFlux. Based on the relationships described above and seen in Figure 10, it is logical to assume that in certain ocean basins, the effects of slower wind speeds and larger near-surface moisture gradients offset each other and work to moderate the differences in the latent heat flux.

These findings begin to provide key context for why differences in evaporation depiction exist between products, as well as context for determining the influence of evaporation on the overall magnitude of water cycle closure over oceans. As noted previously, the atmospheric branch of the hydrologic cycle begins to fall out of closure in the West Pacific in the early 2000s. Within the comparison of evaporation products shown in Figure 2, however, it is obvious that evaporation does not appear to exhibit any significant temporal trends in any of the basins. Given the warming SSTs, especially in the West Pacific, a corresponding increase in evaporation magnitude would be expected based on the bulk flux relationship in Equation 2. However, this does not appear to be present in the West Pacific, as the magnitude of evaporation in all three products remains relatively stable temporally, despite the warming SSTs. Based on Equation 1, this would suggest that either near-surface winds or moisture are compensating for this increase in SST.

3.2: Precipitation

Over the oceans, in-situ observations of precipitation are not feasible, especially on large spatial and temporal scales. Despite ground-based observations existing at several isolated

locations in the Pacific, satellite observations of precipitation provide the necessary spatial and temporal coverage required for budget studies. However, as discussed previously, there is no single one-size-fits-all approach for retrieving precipitation information from satellite observations. While the GPROF algorithm itself is fairly commonly used, different products prioritize precision and accuracy differently, and therefore may give different results depending on precipitation type or the area in which the precipitation was observed. While these differences are inconvenient and can provide a false sense of confidence if the nuances in the product are not considered, the differences themselves can also illuminate characteristics about the underlying environment.

Within this study, monthly average values of precipitation were compared among the observational IMERG version 6, GPCP version 2.3, and GPCP 1-degree daily (1DD) products, as well as values from the ERA-5 and MERRA-2 atmospheric reanalysis products. This comparison was previously shown in Figure 3. Several interesting patterns emerge when analyzing the differences between basins. Throughout all basins, both versions of GPCP generally produce the smallest magnitude of precipitation of all products. This is most pronounced in the West Pacific, where GPCP precipitation is often nearly 2 mm/day smaller than the other products. This is also the case in the Indian Ocean, Atlantic Ocean, and Eastern Pacific basins, although to a much lesser degree than in the West Pacific. Also interesting to note here is the varying relationship between the values produced by each of the reanalyses. If, for example, a shift in the relationship between products occurs, it may suggest either a change in the environment, or a change in observational input to the assimilation scheme or model artifacts within the reanalysis. Within the time series shown in Figure 3, ERA-5 and MERRA-2 are in generally good agreement with one another in all basins except the Central Pacific. Within the

Central Pacific, ERA-5 precipitation is larger than MERRA-2 by approximately 1 mm/day throughout the beginning of the series, until the two reanalyses come into better agreement after 2010. Taken as a whole, the reanalysis products generally produce larger magnitudes of precipitation than the observational products in most basins, which is a similar pattern observed in the comparison of evaporation magnitude between reanalysis and observational products. In terms of the observational products, both versions of GPCP are in relatively good agreement with each other in all basins. Both versions are also in good agreement with IMERG in the Central and East Pacific, as well as in the Atlantic Ocean. Notably though, IMERG depicts larger magnitudes of precipitation than GPCP in the Indian Ocean and the West Pacific. This can be seen more clearly in Figure 11, which is a two-dimensional histogram comparing the precipitation depicted by GPCP 1DD and IMERG at each time point within the period of study. Within Figure 11, it is clear that IMERG magnitudes of precipitation are larger than GPCP for all months in the West Pacific, and for nearly all months in the Indian Ocean. The largest differences between the two products also appear to correspond to the largest rain rates in both of these basins. Another point of interest here is the fairly dramatic differences between the patterns in the West Pacific and the Central Pacific.

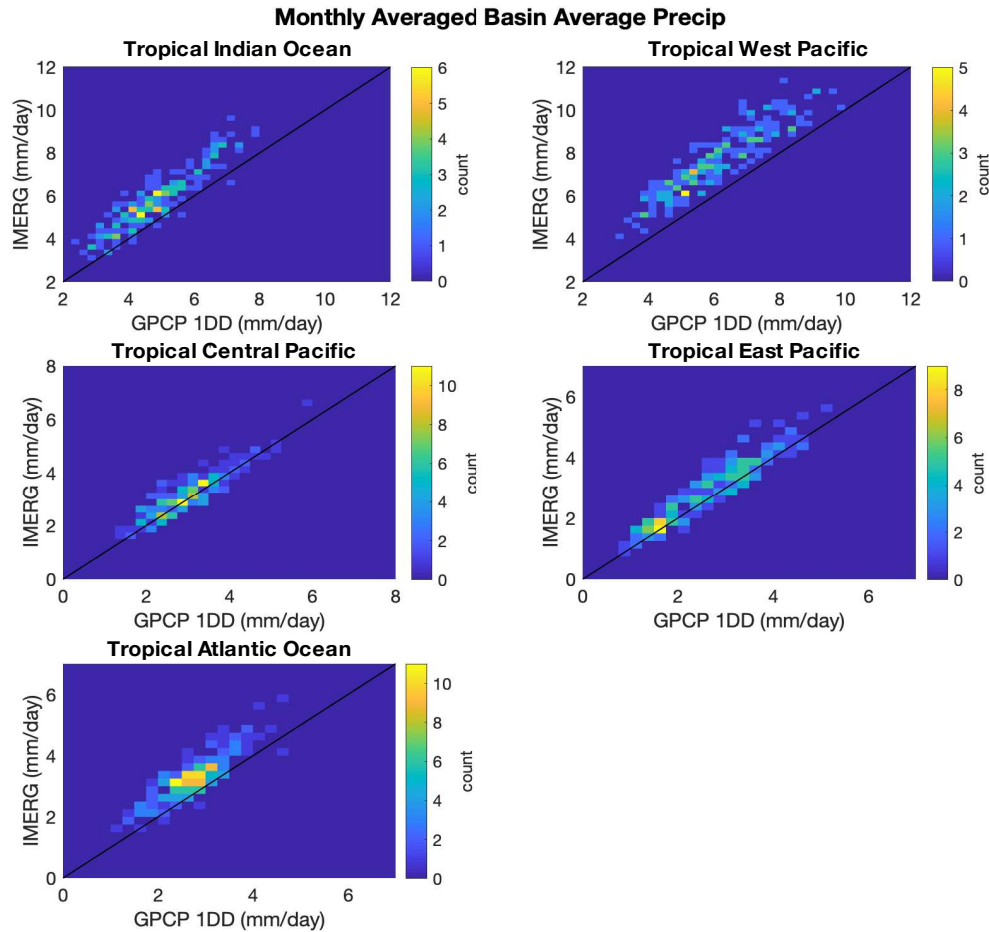


Figure 11: Two-dimensional histogram comparison of precipitation as depicted by GPCP 1DD and IMERG. Each count corresponds to a single monthly average precipitation rate within the period of study.

In contrast to the West Pacific, GPCP and IMERG are in relatively good agreement in the Central Pacific. This may be partially explained by the difference in precipitation types, with the Central and Eastern Pacific dominated by shallower convection, while the Atlantic has some deep, and the Indian and Western Pacific warm pool dominated by deep convective precipitation. This is suggestive of differences between products likely being related to the physical character of precipitation rather than the magnitude.

To obtain greater context into the differences between the various precipitation products, the month-to-month change (dP/dt) was calculated from a standardized version of each time series. The results for the West, Central, and East Pacific are shown in Figure 12.

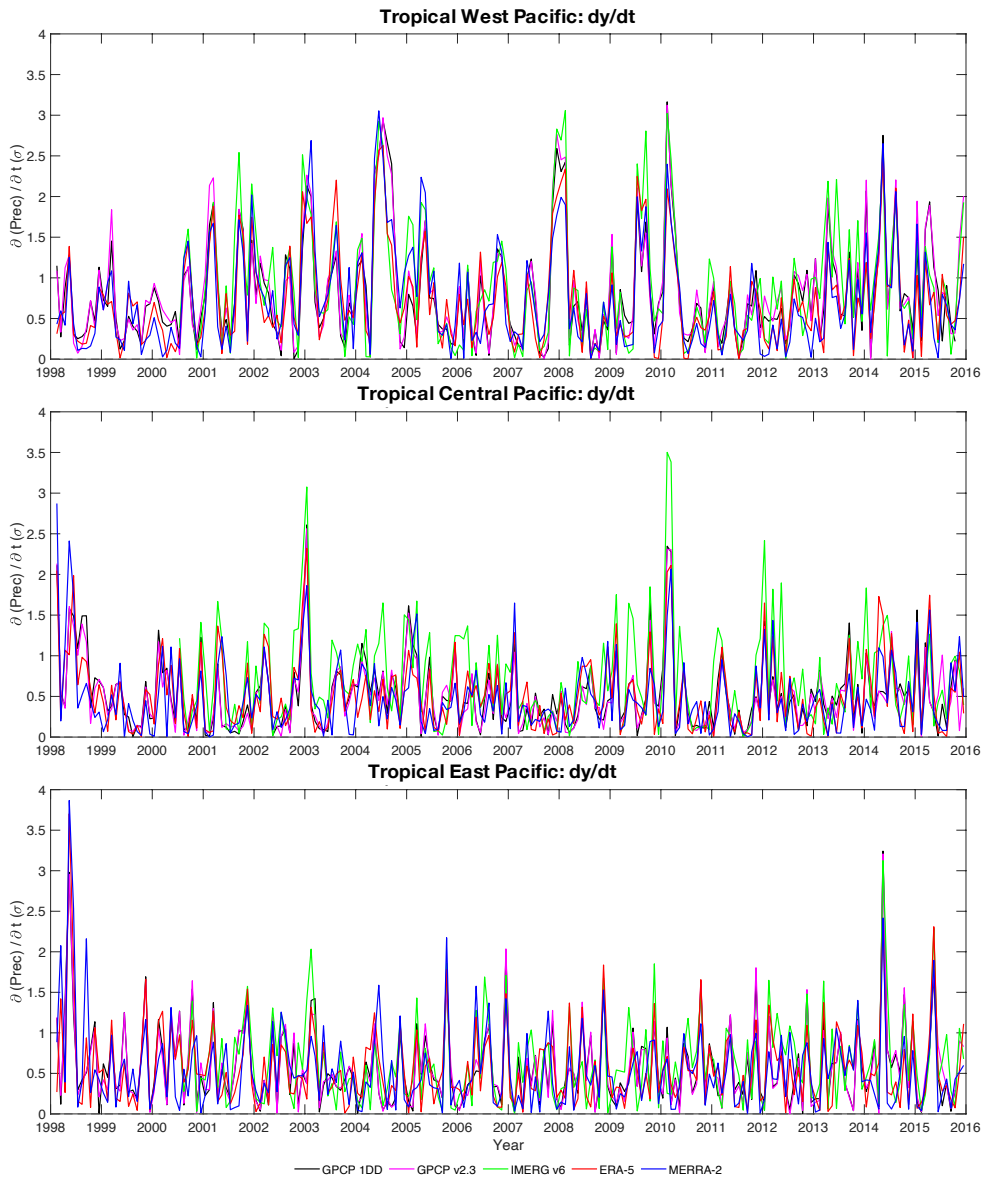


Figure 12: Time series of month-to-month change (dy/dt) of monthly average precipitation for the West Pacific (top), Central Pacific (middle), and East Pacific (bottom)

This is a way to visualize the short-term variability in each product and compare the relationships between products across basins. From Figure 12, it is clear that there are fairly

obvious differences between the Pacific basins. In the West and East Pacific, month-to-month variability is relatively similar amongst the products. In contrast, IMERG dP/dt is consistently larger than the other products in the Central Tropical Pacific. This can be seen more clearly in Figure 13, which shows the average dP/dt for each product over the entire length of the period of study. The largest magnitude of dP/dt is found in the tropical Indian Ocean and the Northern and Southern West Pacific due to the strong seasonality of precipitation in these regions. However, in these basins, IMERG is more or less consistent with the other products. In the tropical West, Central, and East Pacific, dP/dt magnitudes are lower, but the difference between IMERG dy/dt and dy/dt within the other products is significantly larger. Fundamentally, the reason IMERG has larger month-to-month variability is likely because the algorithm responds more strongly to changes in precipitation character than the other products. In other words, because of the focus of IMERG on instantaneous precipitation in contrast to the focus on monthly mean values within GPCP, any physical changes in the environment which alter the character of the precipitation in a

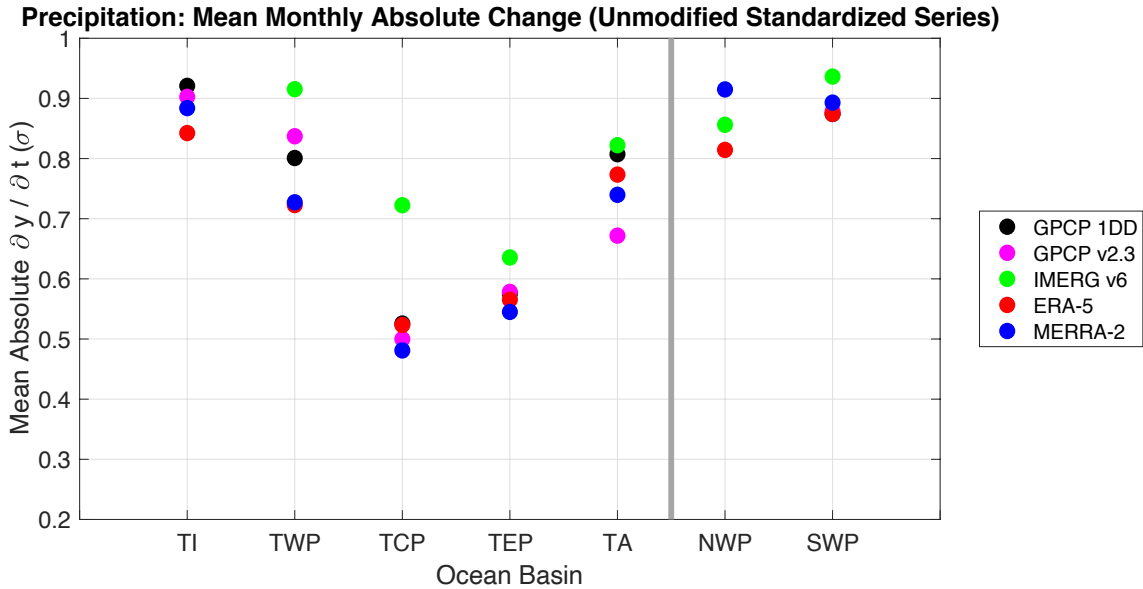


Figure 13: Average dy/dt for all precipitation products over the length of the period of study.

way that results in bias in the passive microwave precipitation retrievals will show up more quickly in IMERG than in other products. This can be the case, for example, during El Nino events when precipitation in the Central Tropical Pacific becomes significantly deeper and more organized.

Remotely-sensed observations of precipitation are far from perfect, and certain observational methods are prone to bias depending on the physical properties of the precipitation being observed. Henderson et al. (2017, 2018) investigated the biases associated with rain rates retrieved from the TRMM Microwave Imager (TMI) using GPROF, finding a fairly robust correlation between El Nino/Southern Oscillation (ENSO) phase and TMI bias. In that work, rain rates retrieved from TMI using GPROF were found to overestimate precipitation during warm SST periods associated with El Nino and underestimate during cool SST periods associated with La Nina. Fundamentally, this was found to result from a change in mean convective state during each respective ENSO period (Henderson et al. 2018). During El Nino, warm SSTs correspond to an increase in the fraction of precipitation resulting from organized convective systems. Within these organized systems are large areas of anvil cloud and deep stratiform precipitation (Elsasser et al. 2010). Henderson et al. (2017, 2018) have shown that GPROF overestimates precipitation in cases of large stratiform rain fraction, as is the case with large organized convective systems. During La Nina events where SSTs are anomalously cool, isolated convection is favored, with a significantly reduced stratiform rain fraction relative to El Nino events. GPROF tends to underestimate precipitation in cases of isolated convective cores, and thus precipitation from GPROF-based algorithms is expected to be biased low during La Nina events. While the study by Henderson et al. (2018) focused only on GPROF biases that underpin the IMERG algorithm, such biases are likely present in other microwave algorithms as the

underlying physics are similar for most retrieval schemes. If precipitation biases are correlated with mean convective state, which is in turn correlated with SST, an analysis of how precipitation partitioning between convective states varies with time should provide insight into the overall influence of precipitation on the magnitude of closure. This will be discussed further in section 4.

3.3: Atmospheric Water Vapor Flux Divergence (divQ)

The final critical component of the atmospheric branch of the hydrologic cycle is the transport of water vapor within the atmosphere. Within the atmospheric water budget framework, the quantity used to represent this is the water vapor flux divergence (divQ). As discussed previously, for this variable we rely solely on atmospheric reanalysis products. Analysis of the differences between reanalysis depictions in each basin will provide context in which to analyze the lack of closure seen in the West Pacific.

Figure 14 displays comparisons between ERA-5 and MERRA-2 depictions of divQ for each basin. Here we see that ERA-5 and MERRA-2 are in relatively good agreement for all basins except the West Pacific. Within the West Pacific, bias between ERA-5 and MERRA-2 is largest for the smallest magnitudes of divQ, whereas the reanalyses are in better agreement for larger negative magnitudes. From Figure 4, it is clear that throughout much of the time series, there is a consistent bias between ERA-5 and MERRA-2. Prior to 2010, ERA-5 and ERA-Interim produce larger magnitudes of moisture convergence than MERRA-2. There are periods where the products are in better agreement such as late 2002, late 2006, and 2009 through 2010, which correspond to El Nino periods. Also of significant interest in this time series is an inflection point around the year 2010, after which ERA-5 and MERRA-2 depictions of divQ come into much better agreement with one another. Before 2010, the difference between ERA-5

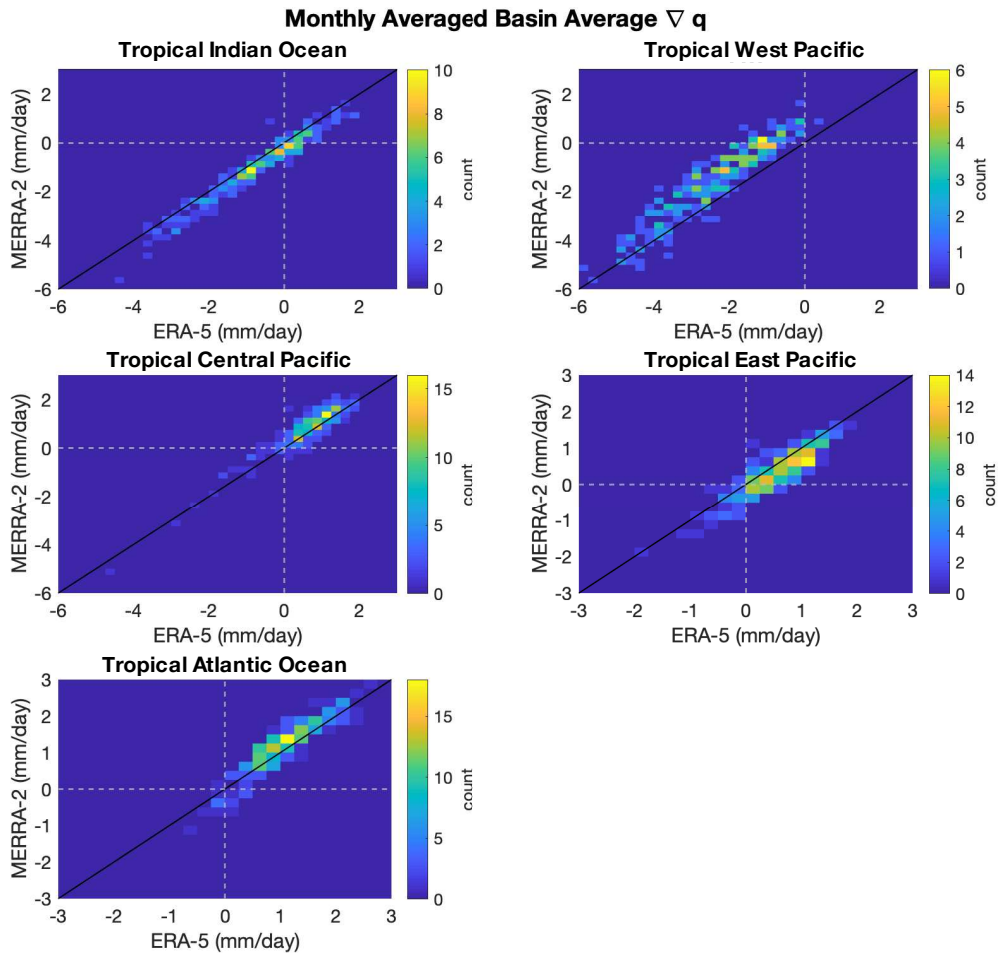


Figure 14: Two-dimensional histogram comparison of $\text{div}Q$ depictions from ERA-5 and MERRA-2 for each basin. Each count corresponds to a single monthly average precipitation rate within the period of study.

and MERRA-2 magnitudes is sometimes nearly 2 mm/day, whereas after 2010 this difference is on the order of 0.5-1 mm/day. While ERA-5 and MERRA-2 come into better agreement after 2010, ERA-Interim retains a similar magnitude of bias relative to MERRA-2 after 2010 as before. This temporal evolution and inflection point near 2010 are only present in the West Pacific basin. This is illustrated in Figure 15, which compares the numerical difference between ERA-5 and MERRA-2 $\text{div}Q$ for each basin. The difference between the West Pacific and all other basins is clearly visible here. The West Pacific is the only basin where the ERA-5 and

MERRA-2 difference is rather large before 2010 before reducing significantly after 2010. All other basins maintain a stable bias between the two products throughout the entirety of the time series.

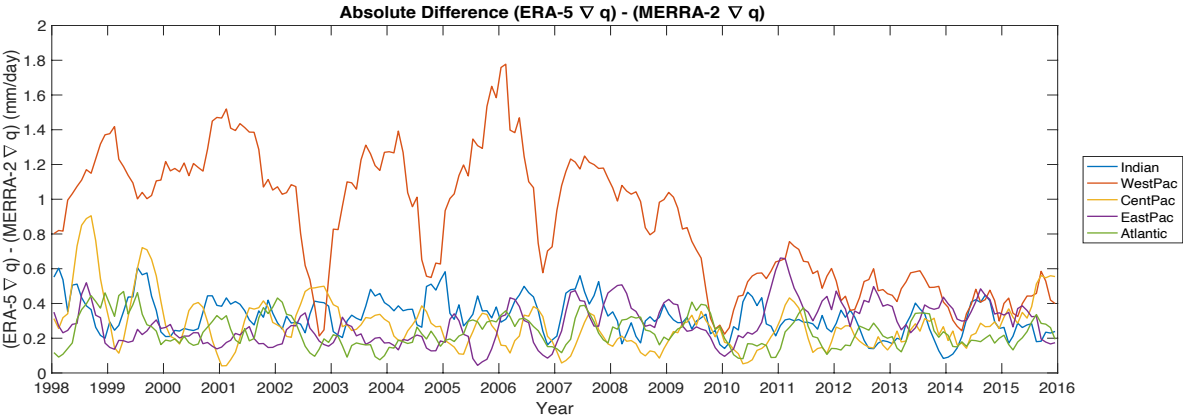


Figure 15: Comparison of the difference between ERA-5 and MERRA-2 depictions of divQ among all basins.

The unique pattern of divQ evolution limited to the West Pacific invites further study into the underlying reasons behind this behavior. Understanding the differences between ERA-5 and MERRA-2 and how they change after 2010 may provide insight into the evolving lack of closure which is similarly limited to the West Pacific, and may be helpful for determining the influence that divQ has on the overall closure magnitude. The two components governing divQ are wind and moisture. Since divQ is a vertically integrated quantity, analyzing the temporal evolution of wind and moisture at multiple levels should help identify the cause of the 2010 divQ inflection point. Figure 16a shows the raw time series comparison between ERA-5 and MERRA-2 depictions of divQ over the West Pacific.

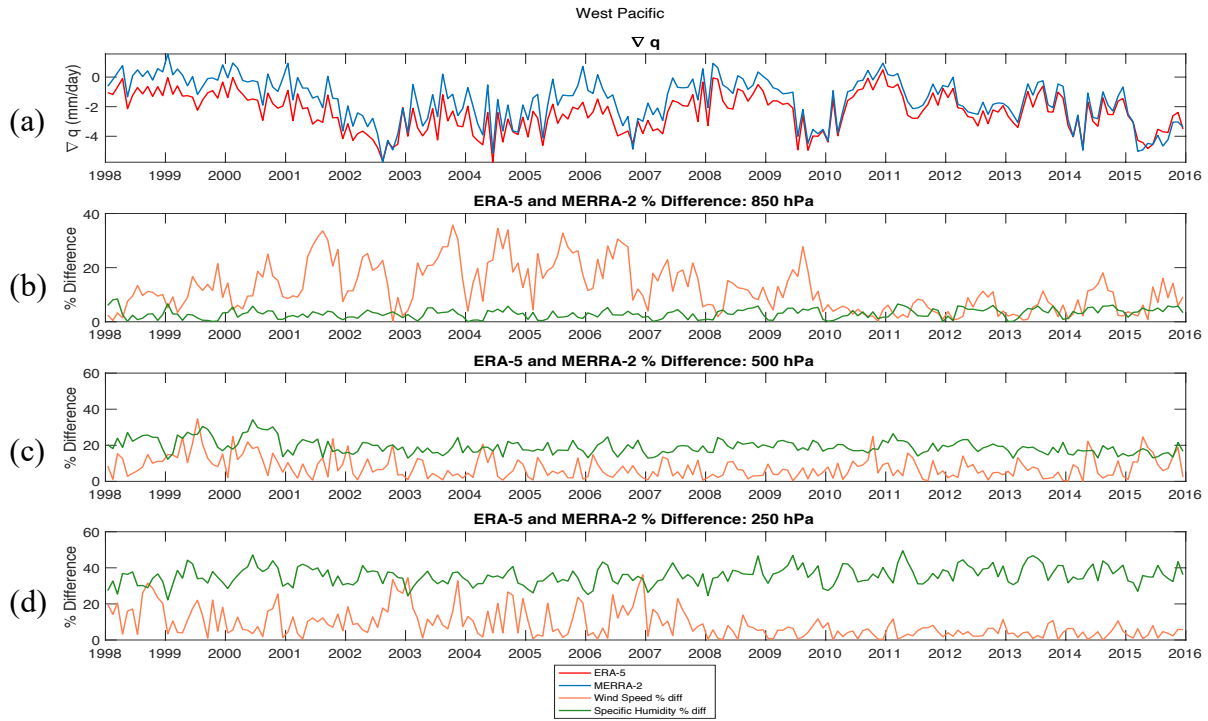


Figure 16: (a) comparison of ERA-5 and MERRA-2 ∇Q magnitudes, percentage difference between ERA-5 and MERRA-2 basin average wind speed and specific humidity at (b) 850 hPa, (c) 500 hPa, and (d) 250 hPa.

In the panels (b), (c), and (d), the percentage difference between ERA-5 and MERRA-2 basin average wind speed and specific humidity are shown at 850 hPa, 500 hPa, and 250 hPa, respectively. At 850 hPa, the inflection point at 2010 is clearly visible in the wind speed differences, where the difference between ERA-5 and MERRA-2 wind speeds decreases dramatically and remains fairly low throughout the rest of the series. In contrast, at this same level, there is no similar inflection point in the percentage difference for specific humidity, as the difference remains low throughout the entire series at 850 hPa. At 500 hPa and at 250 hPa, the percentage difference between ERA-5 and MERRA-2 specific humidity is much higher than at 850 hPa; however, there is again no inflection point visible. Wind speed differences are generally smaller at 500 hPa than at 850 hPa, with no inflection point at 2010 at 500 hPa. At 250 hPa, differences between wind speed depictions are higher prior to 2008, after which they come into

better agreement. However, the presence of a small inflection point here at 2008 does not manifest into the divQ series. This is likely because the very small amount of moisture present at 250 hPa is not large enough to influence overall magnitude of vertically integrated divQ. Therefore, it is logical to conclude that the overall magnitude of vertically integrated divQ is most heavily influenced by lower-tropospheric wind patterns, and an inflection point in the difference between ERA-5 and MERRA-2 lower-tropospheric wind speeds is responsible for the inflection point in the broader divQ differences.

To confirm the dominant influence of lower-tropospheric wind on overall divQ evolution, ERA-5 and MERRA-2 depictions of wind speed and specific humidity were compared at 925, 850, 800, 700, 600, 500, 400, 300, and 250 hPa. Comparisons of specific humidity at these levels generally show a lack of inflection point in the relationship between the two reanalyses. This is shown in Figure 17 for the West Pacific. There is some convergence between products at 700 hPa, but this generally occurs before 2010 and is not reflected at any other level. As a comparison, the same time series for the Central Pacific is shown in Figure 18. Here, there is a similar pattern with no inflection points visible at any level, which is expected given the lack of inflection point in the broader divQ series either.

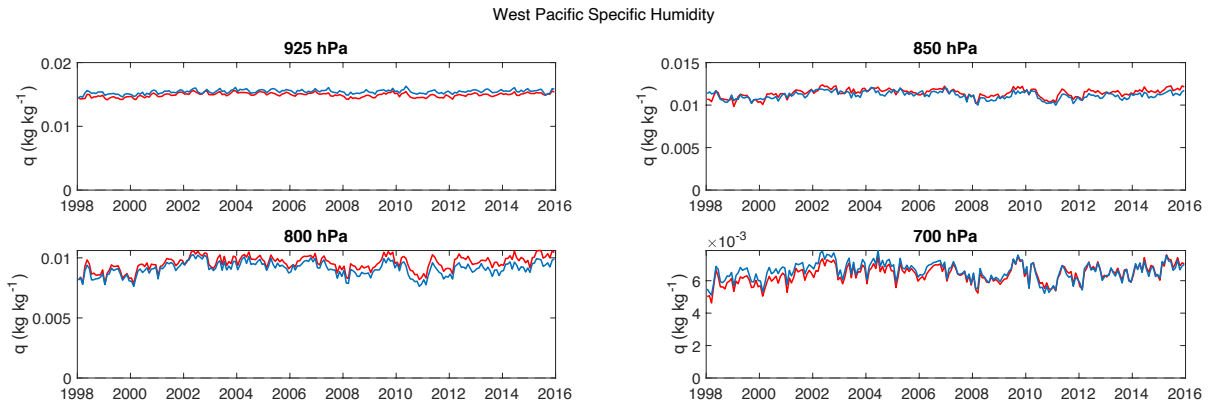


Figure 17: Comparison of basin average specific humidity at levels ranging from 925 to 700 hPa in the West Pacific for ERA-5 (red) and MERRA-2 (blue) (Upper levels are omitted).

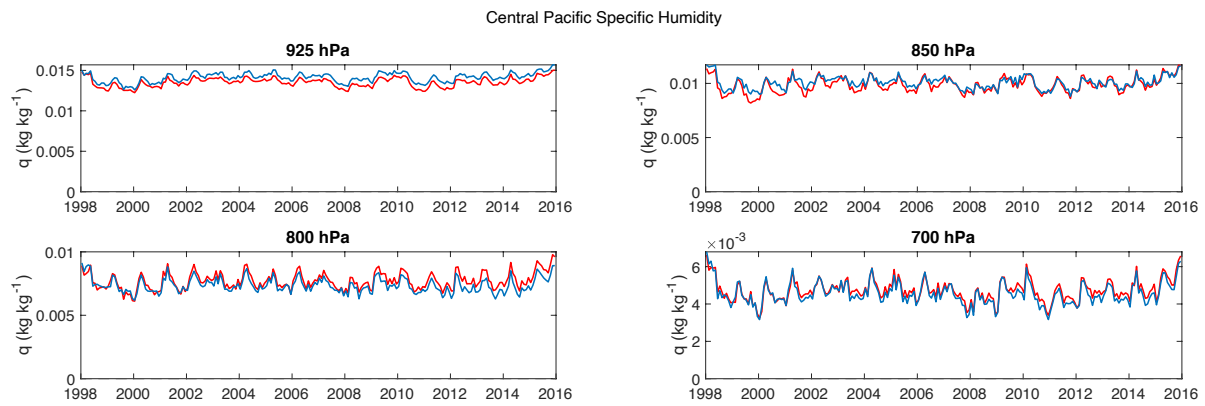


Figure 18: Comparison of basin average specific humidity at levels ranging from 925 to 700 hPa in the Central Pacific for ERA-5 (red) and MERRA-2 (blue) (Upper levels are omitted).

Similar comparisons were also plotted for the zonal wind component, meridional wind component, and total wind speed. These are shown in Figure 19 for the West Pacific and Figure 20 for the Central Pacific.

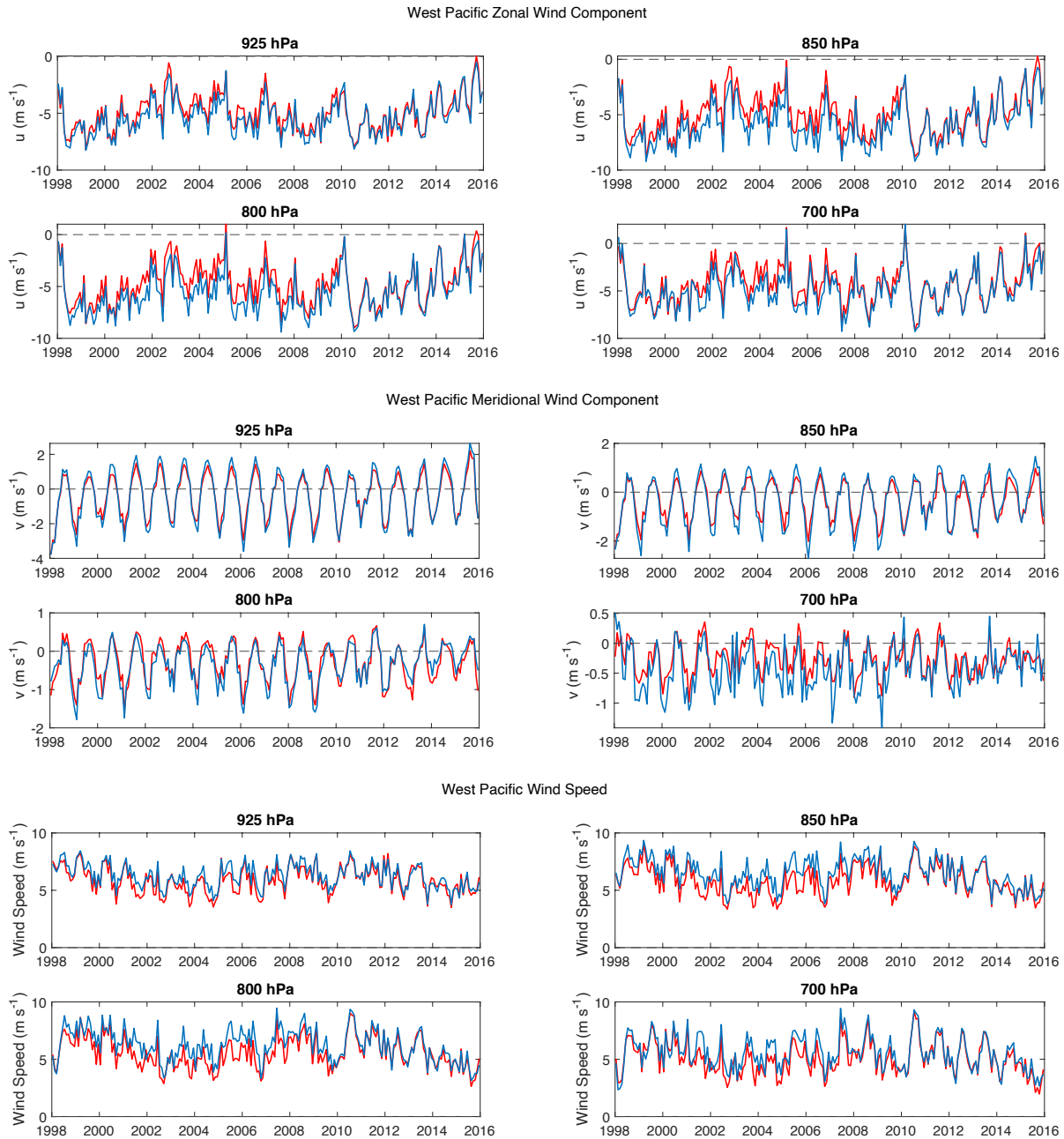


Figure 19: Comparison of basin average u -wind, v -wind, and total wind speeds at levels ranging from 925 to 700 hPa in the West Pacific for ERA-5 (red) and MERRA-2 (blue) (Upper levels are omitted).

Within the West Pacific, the 2010 inflection point is clearly visible in the u -wind component, where at low levels the two products come into dramatically better agreement with one another after 2010. The v -wind component, by contrast, does not appear to have a similar inflection point as the u -wind component. Since zonal wind magnitude is much larger than

meridional magnitude at these tropical latitudes, the zonal wind patterns dominate and the inflection point in zonal winds is reflected in the total wind speed.

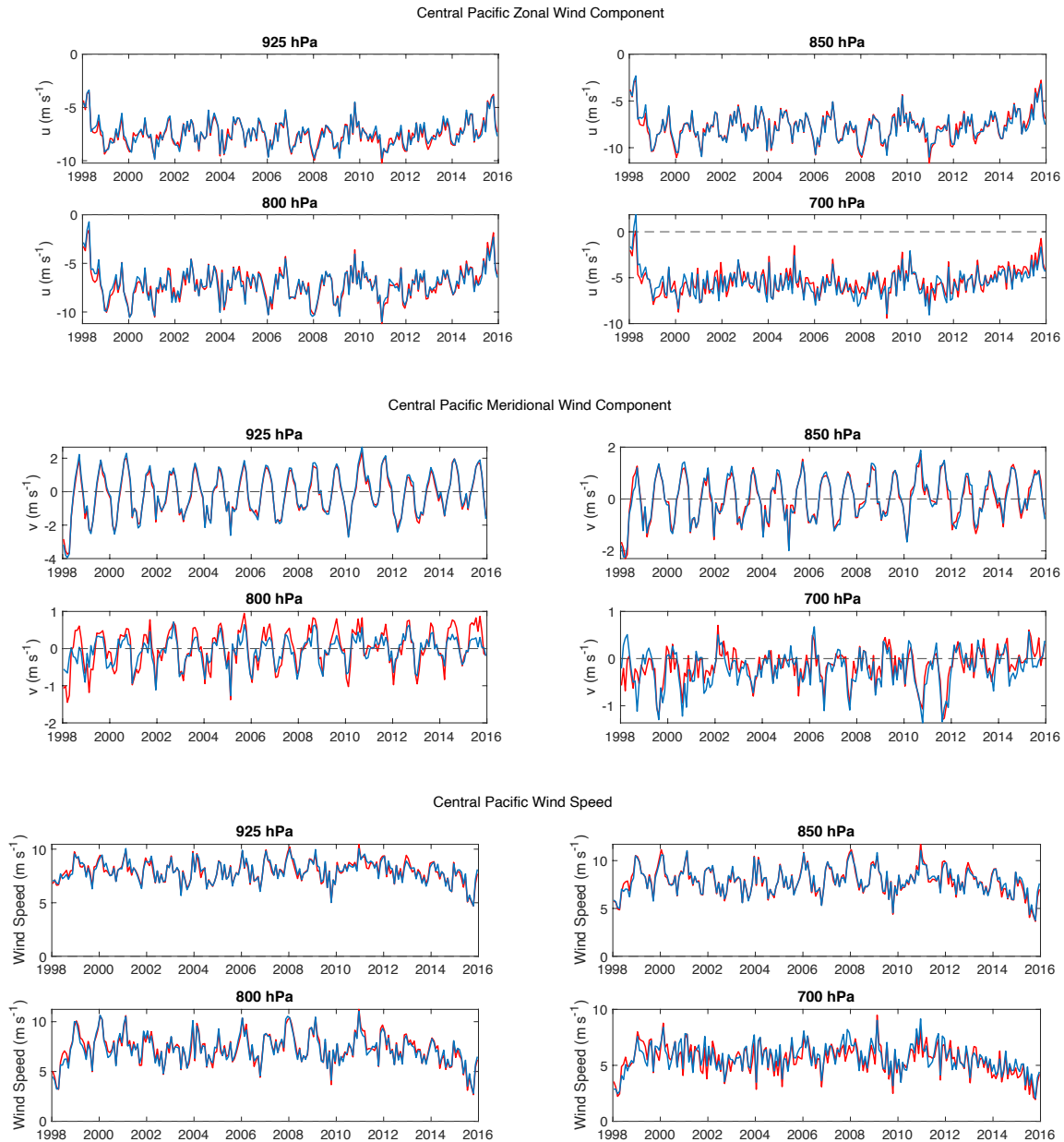


Figure 20: Comparison of basin average u -wind, v -wind, and total wind speeds at levels ranging from 925 to 700 hPa in the Central Pacific for ERA-5 (red) and MERRA-2 (blue) (Upper levels are omitted).

The differences between ERA-5 and MERRA-2 winds in the Central Pacific reflect patterns seen in Central Pacific moisture. That is, there are no inflection points in the wind field at any level

over the Central Pacific. Overall, ERA-5 and MERRA-2 are in much better agreement for both wind and moisture in the Central Pacific when compared to the temporally varying patterns seen in the West Pacific.

These results suggest when considering the differences between ERA-5 and MERRA-2 depictions of $\text{div}Q$, lower-tropospheric wind is the most influential variable in determining the overall evolution of $\text{div}Q$. This motivates additional analysis to determine if this inflection point is due to changes in the reanalysis observing system, a model artifact, or related to physical changes in the environment. One way to gain additional insight is to examine the analysis increments output from the reanalysis. MERRA-2 includes analysis increments, which are essentially the difference between the assimilated observational value of a parameter and the model forecast of that same parameter. As such, the analysis increment details the impact within the reanalysis framework of the assimilated observations on the modeled value (Bosilovich et al 2011). The evolution of the analysis increments for vertically integrated moisture content for all basins are shown in Figure 21. From this figure, it is clear throughout all basins that the analysis increment magnitude for moisture does indeed exhibit an inflection point around 2010. After this point, magnitudes come into much better agreement with one another than during the period prior to 2010.

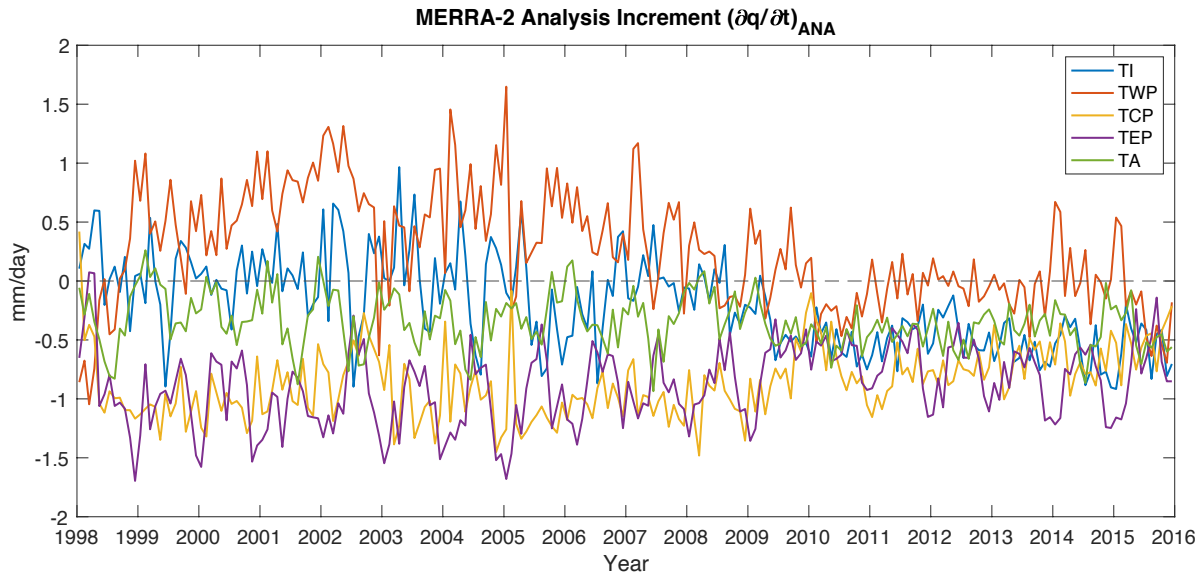


Figure 21: Basin average MERRA-2 analysis increments for vertically integrated moisture for all basins.

When analyzing the analysis increments for u- and v-components of wind (Figure 22), there is also a distinct inflection point in both components at multiple pressure levels. These are most notable at 925 hPa, where after 2010, trends in analysis increments for both u- and v-components appear to stabilize. Inflection points also appear at upper levels at and above 600 hPa, where after 2010, trends in analysis increments appear, in contrast to pre-2010 when trends are minor. Interestingly, analysis increments were generally fairly small at the 850 hPa and 800 hPa relative to other levels for both u- and v-components. The 2010 inflection point also does not appear to be present at these levels, highlighting the importance of the lowest levels of the atmosphere in the determination of overall $\text{div}Q$.

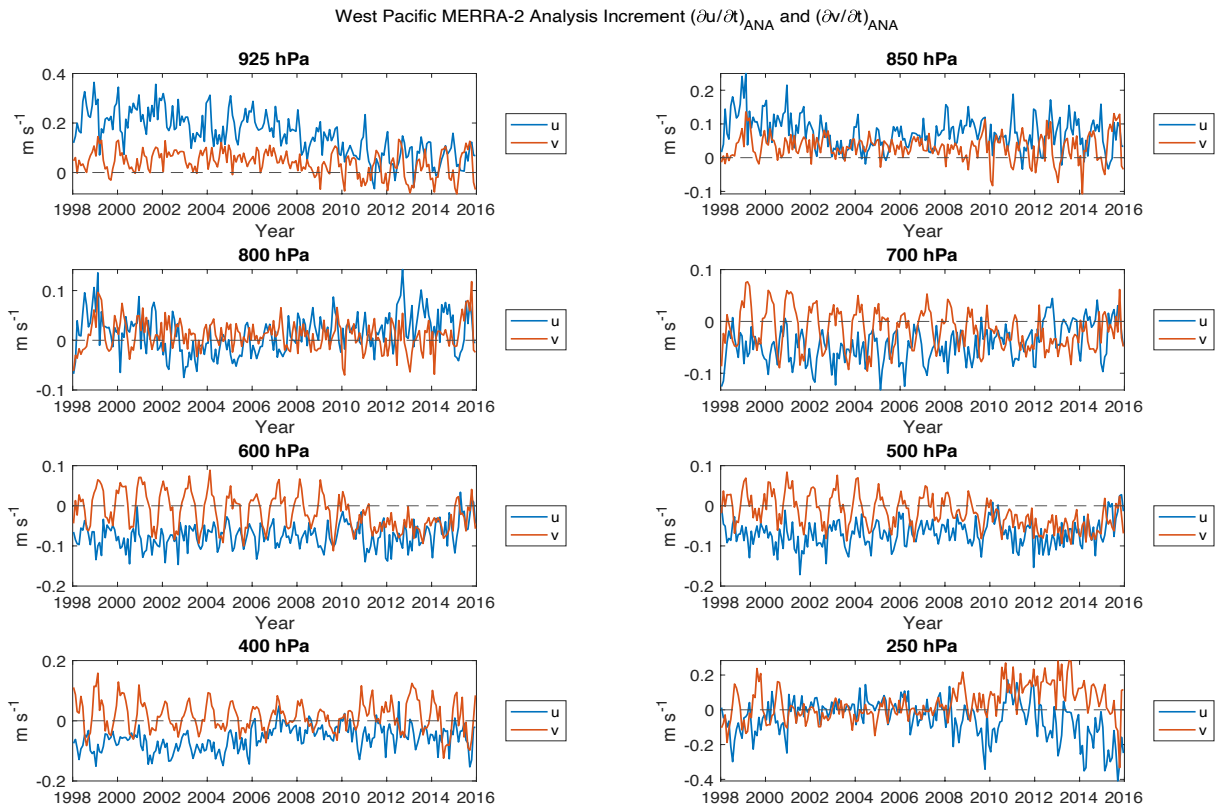


Figure 22: Basin average MERRA-2 analysis increments for u and v wind components at multiple levels for the West Pacific basin.

Overall, it is difficult to directly determine the cause of the 2010 inflection point. Since the underlying model within reanalysis product is fixed, the most likely cause behind the sudden convergence of $\text{div}Q$ magnitudes between ERA-5 and MERRA-2 in the West Pacific is an artifact resulting from a change in the assimilated observations occurring in the vicinity of 2010. This time period corresponds with the end of the assimilation of observations from SSMI, which affects characterizations of water vapor within the atmosphere. Regarding the overall effects of $\text{div}Q$ on closure, the inflection point after which the reanalyses come into better agreement does not line up precisely with the period of lack of closure in the West Pacific. However, the fact that this pattern of $\text{div}Q$ evolution only exists in the West Pacific and is anomalous relative to the other basins does suggest that the depiction of $\text{div}Q$ does have an effect on the overall magnitude

of closure which will be discussed further in the next section. Based on the inflection point analysis within the context of trends in divQ, anomalous behavior in the vicinity of 2010 appears to be limited to MERRA-2. ERA-5 representations of divQ seem to be more consistent over time, suggesting that ERA-5 is better suited for long-term studies of hydrologic cycle closure.

3.4: Overall Magnitude of Water Cycle Closure

To this point, analysis has been limited to the evolution of the individual components of the atmospheric branch of the hydrologic cycle and the relationship between depictions from different products. The analysis of each component and the products used to represent it has demonstrated the differences in magnitude, variability, and trends among products, some of which are significant but difficult to diagnose without the existence of absolute “truth” values with which to compare. In this section, we demonstrate the importance of product choice when analyzing the evolution of hydrologic cycle closure, and attempt to determine the influence of each respective component on the overall magnitude of hydrologic cycle closure.

In this work, closure is defined and referred to as the quantity $\text{divQ} - (E - P)$. As such, the magnitude of closure depends on which products are chosen for E, P, and divQ. To visualize the impact of varying these source products, the magnitude of closure was calculated four separate times; using GPCP for P and ERA-5 for divQ, using GPCP for P and MERRA-2 for divQ, using IMERG for P and ERA-5 for divQ, and using IMERG for P and MERRA-2 for divQ. SeaFlux was used for evaporation in all calculations; as previously discussed, some differences in the overall magnitude between evaporation products were observed, but trends were limited to precipitation and divQ. These time series of closure are shown in Figure 23 for the West and Central Pacific basins. The West and Central Pacific regions are the focus of this figure as they demonstrate the largest contrast in closure behavior between differing basins. It

should be noted that other basins, particularly the Indian Ocean, maintain consistently good closure throughout the period of study regardless of the products used in its calculation.

When the precipitation source is held constant and the divQ source is changed between ERA-5 and MERRA-2, there is a notable change in the time series of closure magnitude in the

$$\text{Closure} = \nabla q - (E - P)$$

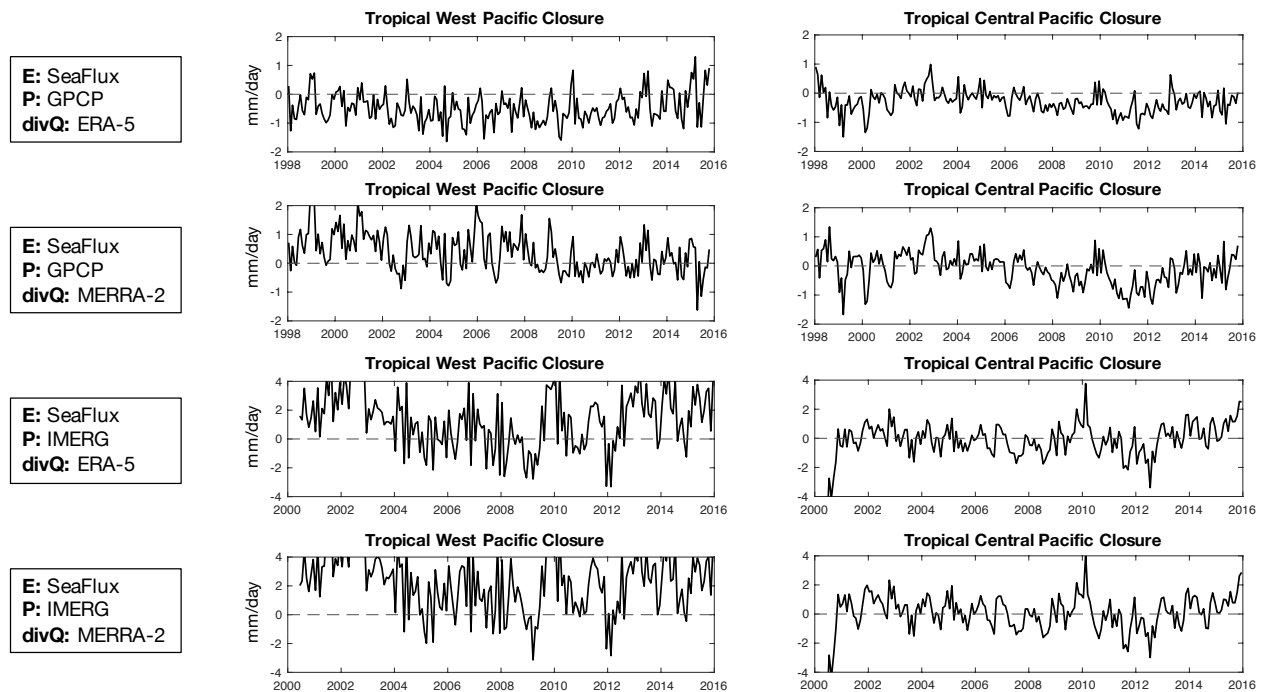


Figure 23: Comparison of closure magnitude when using different products as sources of evaporation, precipitation, and divQ. Results for the Tropical West Pacific (TWP) are displayed in the left column, and results for the Tropical Central Pacific (TCP) are displayed on the right.

West Pacific. With ERA-5 used as the source of divQ, the West Pacific falls out of closure early on, before slowly starting to regain closure after 2010. This is the pattern seen in prior work from Brown and Kummerow (2014), and the time series exhibits a relatively smooth and consistent trend throughout the period of study with no major sudden jumps in magnitude. With SeaFlux and GPCP used as the sources for evaporation and precipitation, respectively, in addition to ERA-5 being used as the source for divQ, this is to be expected due to these three products being

generally regarded as the most stable over time. However, when MERRA-2 is used as the source for $\text{div}Q$, the time series of closure magnitude exhibits a markedly different character which confirms the presence of a reanalysis artifact which in practical terms disqualifies the use of MERRA-2 in studies of closure during this specific time period. Within Figure 19, this is seen in the second panel from the top in the leftmost column. Here, it is obvious that an inflection point exists in the time series of closure magnitude near the year 2010. This is an artificial jump in closure magnitude induced by the aforementioned changes in the assimilation of observations into MERRA-2 around this time. Practically, the presence of this inflection point confirms that MERRA-2 is not suitable to be used in closure studies in this region during this time period, as its use introduces an artificial jump to the magnitude of closure. This jump suggests that closure suddenly returns to balance in the year 2010, when in reality it is more likely that the return to closure is more of a slow and steady trend as depicted by the series when ERA-5 is used as the source for $\text{div}Q$. The physical mechanisms which are likely responsible for the trends in closure in the West Pacific are explored in Chapter 4.

In contrast to the West Pacific, there is very little change in the closure series in the Central Pacific when $\text{div}Q$ is switched between ERA-5 and MERRA-2, which further confirms the artificial nature of the inflection point seen in the West Pacific when MERRA-2 is used as the source for $\text{div}Q$. To analyze the effects of switching the source of precipitation from GPCP to IMERG, $\text{div}Q$ source was kept constant and while precipitation source varied in the calculation of closure magnitude. This is also shown in Figure 19. When precipitation is switched between GPCP and IMERG, the differences in magnitude of closure in the West Pacific are quite dramatic for both sources of $\text{div}Q$. When IMERG is used for precipitation, the magnitude of the lack of closure is much larger than when GPCP is used for precipitation and short term

variability is also much larger due to the differences in mission between GPCP and IMERG. In both cases of divQ source, the West Pacific does not achieve consistent closure at all when IMERG is used for precipitation. This is a large contrast to the magnitude of closure when GPCP is used for precipitation, during which the overall series is also far more stable. Again, the Central Pacific exhibits a very different pattern than the West Pacific. Whereas the West Pacific closure series changes dramatically when the precipitation source is switched between IMERG and GPCP, the changes in the Central Pacific are relatively minor. These results again illustrate the stark differences between the West Pacific and other basins, both in terms of lack of closure overall, as well as the very large impact that a switch in input products has on the overall magnitude of the lack of closure. These results emphasize the importance of product choice when analyzing the magnitude of hydrologic cycle closure, as the character of changes in closure magnitude can indicate the physicality of these changes. That is, if closure magnitude changes suddenly, as is the case when MERRA-2 is used as the source for divQ, this is not likely a physical change. In contrast, the depiction of closure magnitude when ERA-5 is used as the source for divQ is much more likely to be physical, as it is more gradual. This likely reflects a physical change in the environment which slowly evolves over time.

CHAPTER 4: DISCUSSION AND CONCLUSIONS

4.1: Summary of Differences between Products

A major goal of this work was to characterize and improve our understanding of the temporal stability of the products used to characterize the hydrologic cycle, within the context of an evolving lack of hydrologic cycle closure in the West Pacific Ocean. This lack of closure was found to be limited to the West Pacific for unknown reasons; therefore a comprehensive analysis of the individual components of the atmospheric branch of the hydrologic cycle was conducted, including ocean evaporation, precipitation, and water vapor flux divergence ($\text{div}Q$). For each of these components, multiple independent observational and model-based products are available, and these products frequently depict variables quite differently from one another.

Depictions of evaporation exhibited similar patterns across basins, with a consistent bias present between magnitudes depicted by observational products and magnitudes depicted by reanalysis products. In all basins studied, magnitudes of evaporation depicted by reanalysis products always exceeded magnitudes depicted by observational products. Useful insight regarding the differences between products was obtained, with findings that reanalysis products appear to simulate a near-surface layer which is too dry, resulting in an over-simulation of evaporation compared to observational products. Regarding temporal variability, evaporation was found to be the most stable variable temporally across all basins, and despite ocean surface warming throughout the period of study over multiple basins, evaporation magnitude remained relatively stable over time. Interestingly, both reanalysis products exhibited increased seasonal variability relative to the observational products. This is likely a result of larger seasonal differences in low level wind and moisture within the reanalyses compared to observations.

Evaporation is also notable in general due to the absence of long-term trends in magnitude. This is consistent across all basins and all products studied, and despite generally increasing SSTs in some basins, the magnitude of evaporation remains stable over time. Bias exists between observational depictions of evaporation and reanalysis depictions, but these biases remain nearly consistent over time and therefore manifest as simple offsets in the overall magnitude of closure.

This work generally focused on precipitation products which are purely observational, but which utilize different approaches with different goals in mind. GPCP Version 2 is anchored to a monthly statistical product over oceans that is intended to be more stable over time at the expense of instantaneous rainfall estimates, while IMERG is intended to be a best instantaneous estimate of precipitation at the cost of long-term stability. The difference in precipitation magnitude between GPCP and IMERG was found to be largest in the West Pacific, with a fairly uniform bias between the two products over time. A relatively large bias between GPCP and IMERG also exists in the Indian and Atlantic basins, with the two products in better agreement in the Central and Eastern Pacific. Similar to evaporation, reanalysis depictions of precipitation magnitude are generally larger than observational depictions. These differences between GPCP and IMERG appear to be traceable to changing convective states in tropical oceans, which will be discussed in the following section. Short-term variability also differs considerably between products, most notably between GPCP and IMERG. This is likely a result of the difference in mission goals for the respective products, with GPCP intended to be more stable over time and IMERG intended to represent an instantaneous best estimate. Consequently, IMERG is more variable over time. Comparing variability in precipitation between regions, short-term variability is highest in the regions where the largest seasonality in precipitation exists. This is mainly in the Indian Ocean and the Northern and Southern West Pacific basins. Trends in precipitation

magnitude are mostly consistent between products despite the differences in magnitude. Outside of general seasonality, the only trends which appear in the precipitation series exist in the West and Central Pacific basins, generally on timescales similar to that of the El Nino/Southern Oscillation.

Depictions of divQ magnitude were notable in that differences between products were fairly small in all basins except the West Pacific. In the West Pacific, a notable bias was present between ERA-5 and MERRA-2 during the beginning of the period of study. Analysis revealed the presence of an inflection point in 2010, after which ERA-5 and MERRA-2 divQ magnitudes come into much better agreement with one another than during the period prior to 2010. This inflection point was not observed in any other basin and was seen to adversely affect the depiction of closure magnitude when MERRA-2 was used as the source for divQ. In addition, an analysis of the underlying components of divQ was conducted to determine the source and physicality of the 2010 inflection point. Lower-tropospheric wind was found to be the most influential factor on overall divQ magnitude, as trends in reanalysis wind patterns matched trends in reanalysis divQ. Variability of divQ was generally uniform across all products and all basins. Overall, the temporal evolution of divQ in the West Pacific was most anomalous relative to the other basins studied, with the relationship between ERA-5 and MERRA-2 depictions of divQ changing relatively dramatically over time due to the inflection point mentioned previously. It was hypothesized that the 2010 inflection point is likely an artifact resulting from either the underlying model or changes to the observing system. Trends differ between products because the inflection appears primarily in the MERRA-2 data, with ERA-5 appearing more stable over time. The fact that MERRA-2's wind increments also changed drastically around 2010 leads us

to believe that ERA-5 is likely the more stable of the two products and thus appropriate for subsequent closure studies.

In terms of the overall magnitude of closure, the magnitude, variability, and trends of each product and each variable affect the closure in varying ways. Consequently, the temporal evolution of closure and the degree to which the hydrologic cycle appears to close are highly dependent on which products are chosen for evaporation, precipitation, and divQ. The differences between the magnitude, variability, and trends of each product therefore are reflected in the differences between closure magnitude when constructed with varying products. Overall, differences in magnitude of precipitation depicted by GPCP and IMERG has a notable effect on closure evolution, mainly in the West Pacific. When the source of precipitation is switched between these two products, variability and lack of closure increases when IMERG is used. In contrast, the overall series of closure is more stable when GPCP is used for precipitation.

4.2: Implications on Magnitude of Closure

Many of the most notable differences between products, specifically precipitation and divQ, were found to be confined only to the West Pacific basin. Despite the fact that there are relatively large differences between observations and reanalysis in terms of variable magnitudes, most basins outside of the West Pacific exhibit relatively good closure regardless of specific product choice. Practically, the significant differences between closure in the West Pacific depending on choice of divQ and precipitation source invite a deeper exploration into the physical mechanisms within the environment which control these differences and affect the temporal evolution of these variables and overall closure. In the case of divQ, differences between reanalysis depictions are primarily due to the underlying model and differences in how each reanalysis processes changes in observational data networks. Regarding precipitation,

observational retrieval algorithms for spaceborne sensors rely on many assumptions, and systematic changes in the physical character of precipitation can affect their accuracy, which consequently can influence the magnitude of closure as well.

When closure magnitude is calculated using SeaFlux for evaporation, GPCP for precipitation, and ERA-5 for divQ (Figure 24), which are the most stable products, the West Pacific basin is a clear outlier where a trend in closure exists. As described previously, the West Pacific basin is unique in that there are distinct differences in closure magnitude depending on which products are used to calculate closure. In addition, the West Pacific basin also is the region where the largest differences between different product depictions of precipitation and divQ exist. The confinement of most major issues to the West Pacific is important, as it allows for the definitive conclusion that satellite drift is not the cause of the evolving lack of closure in the West Pacific. If it was indeed satellite or other observation system drift which was responsible,

$$\text{Closure} = \nabla q - (E - P)$$

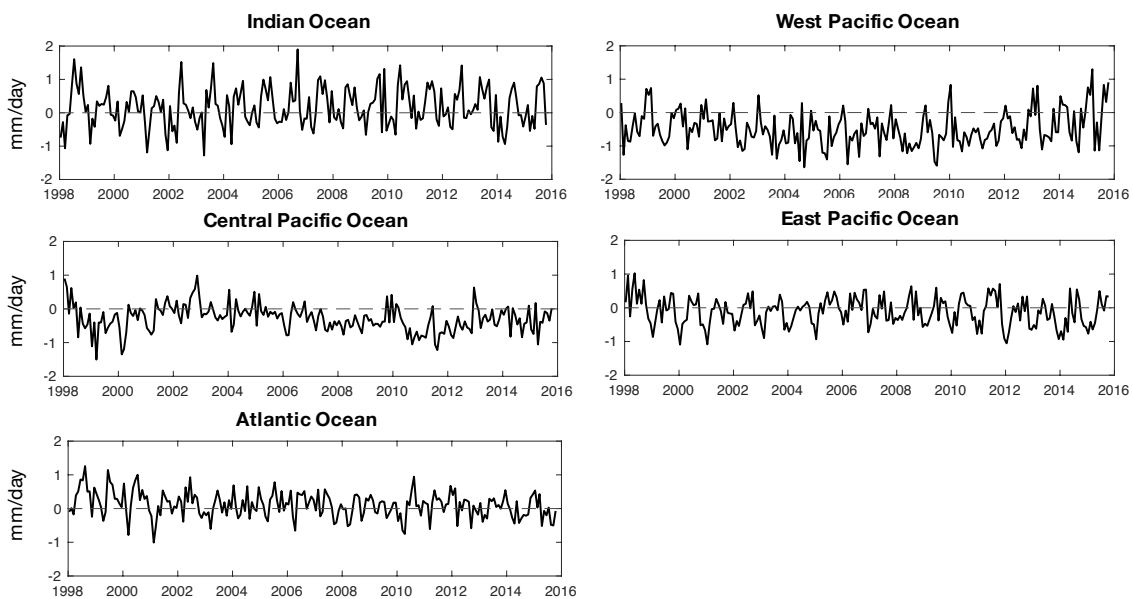


Figure 24: Comparison of closure magnitude using SeaFlux as the source for evaporation, GPCP as the source for precipitation, and ERA-5 as the source for divQ.

there would be noticeable shifts in variable magnitude in other basins as well as the West Pacific, since it is the same satellites and the same instruments which observe the whole globe. Since no comparable trends are present in other basins, it is concluded that satellite drift is not responsible for the trends in closure. This, therefore, indicates that trends in closure in the West Pacific are likely due to changes in the environment specific to the West Pacific basin which impact the accuracy of some or all of the products used to depict the hydrologic cycle.

Instead, we hypothesize that the lack of closure is the result in a change in the physical environment in the West Pacific that leads to biases in the precipitation products. Fundamentally, any observational precipitation retrieval algorithm depends upon a certain set of assumptions about precipitation characteristics used in the construction of the retrieval. These include details such as precipitation inhomogeneity. If, for example, the mean convective state was to change, the assumptions used in the retrieval may no longer be appropriate and biases could be introduced into the individual precipitation products. This is what is hypothesized to have occurred in the West Pacific during the period where the hydrologic cycle falls out of closure. Prior work has given this theory some merit, finding that GPROF tends to overestimate precipitation in cases where there is a large amount of stratiform precipitation, and GPROF tends to underestimate precipitation in cases where there is a reduced stratiform fraction and isolated convective cores dominate (Henderson et al. 2017). While GPCP does not use the GPROF algorithm, it can be speculated that other algorithms, including Wilheit et al., (1990) might have similar biases. Cases where stratiform fraction is higher tend to occur when convective systems are more organized and have large associated anvils, while smaller stratiform fractions tend to occur when convection is more isolated. Therefore, an analysis of mean precipitation character

and the fraction of precipitation resulting from deep organized and deep isolated convection in each basin over time should provide insight into the plausibility of this hypothesis.

To analyze any changes in precipitation character and convective partitioning over time, the temporal evolution of the fraction of precipitation resulting from shallow, deep isolated, and deep organized convection was compared among all basins, using the methods of Elsaesser et al. 2010 and Henderson et al. 2017. The 6-month average time series of fraction of precipitation resulting from deep isolated convection and deep organized convection for the West Pacific is shown in Figure 25.

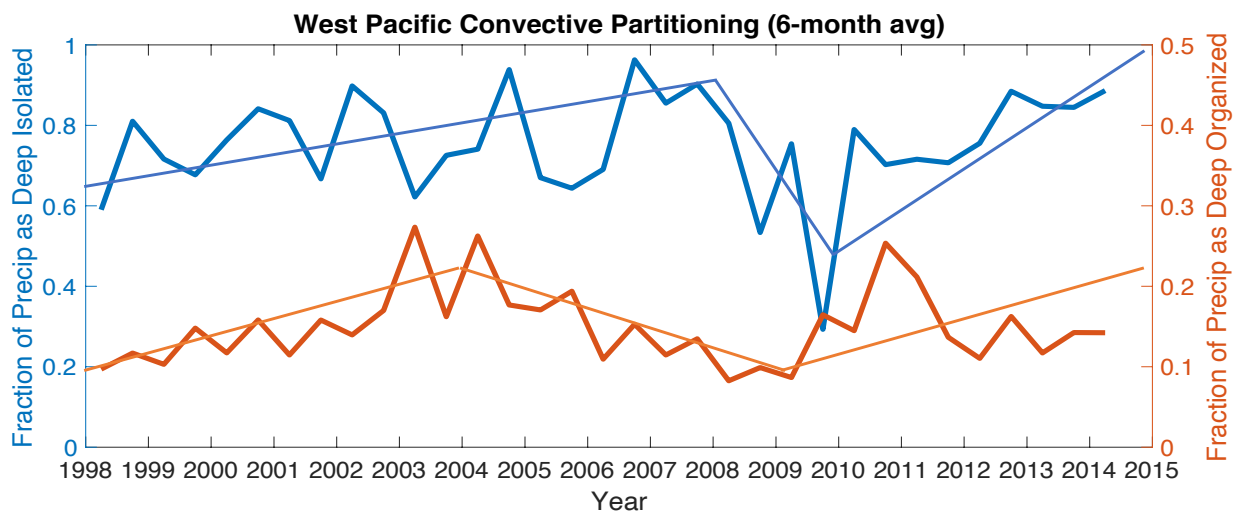


Figure 25: 6-month average of fraction of precipitation resulting from deep isolated convection and deep organized convection for the West Pacific.

The same time series for the Central Pacific is shown in Figure 26. With the effects of both a larger than average fraction of precipitation from deep isolated convection and from deep organized convection in mind, the effects of a temporal shift in these fractions on overall magnitude of closure can be taken into account when attempting to determine the causes of the lack of closure in the West Pacific. In the West Pacific, the components of the hydrologic cycle were found to trend out of closure during the middle of the period of study, before coming back into closure near the end of the period of study. In Figure 25, the fraction of precipitation

resulting from deep isolated convection is generally increasing throughout the period of study. Physically, this would correspond to an increasing underestimation of precipitation by GPROF based on the findings of Henderson et al. (2017). Also in Figure 25, a similar pattern is visible during the beginning of the series as the fraction of precipitation resulting from deep organized convection increases. However, this trend appears to reverse around the year 2004, after which the deep organized convective fraction appears to remain steady and then decrease. Furthermore, the deep organized convective fraction reverses trend yet again towards the end of the timeseries, trending upward. According to the findings from Henderson et al. (2017), this would result in an increasing overestimation of precipitation by GPROF until about 2004, followed by a period of decreasing overestimation, followed by a final period of increasing overestimation.

This would suggest that during the beginning of the series, the underestimation of precipitation from deep isolated convection balances the overestimation of precipitation from deep organized convection as the fraction for both appears to increase uniformly. Therefore, the ratio between the two fractions remains fairly constant. In contrast, after the year 2004 the fraction of precipitation from deep organized convection begins to decrease. This results in the underestimation of deep isolated precipitation no longer balancing the overestimation of deep organized precipitation. Thus, the ratio between the two fractions is no longer constant with time, resulting in a residual near the middle of the series. This lack of balance between the fraction of precipitation resulting from deep organized and deep isolated convection matches up with the evolving lack of closure in the West Pacific, and seems to explain the evolving lack of closure. Moreover, the return to general closure at the end of the time series matches with the ratio of deep isolated to deep organized convection returning to a generally constant value with time.

The same temporal evolution is shown for the Central Pacific in Figure 26, the East Pacific in Figure 27, the Indian Ocean in Figure 28, and the Atlantic Ocean in Figure 29. Since TRMM data is limited to the tropics, this analysis cannot be conducted for the midlatitude basins. Contrasting the evolution of convective organization in the West Pacific with the evolution in other basins provides insight into the plausibility that the changing ratio between isolated and organized convection may be responsible for the lack of closure within the West Pacific basin.

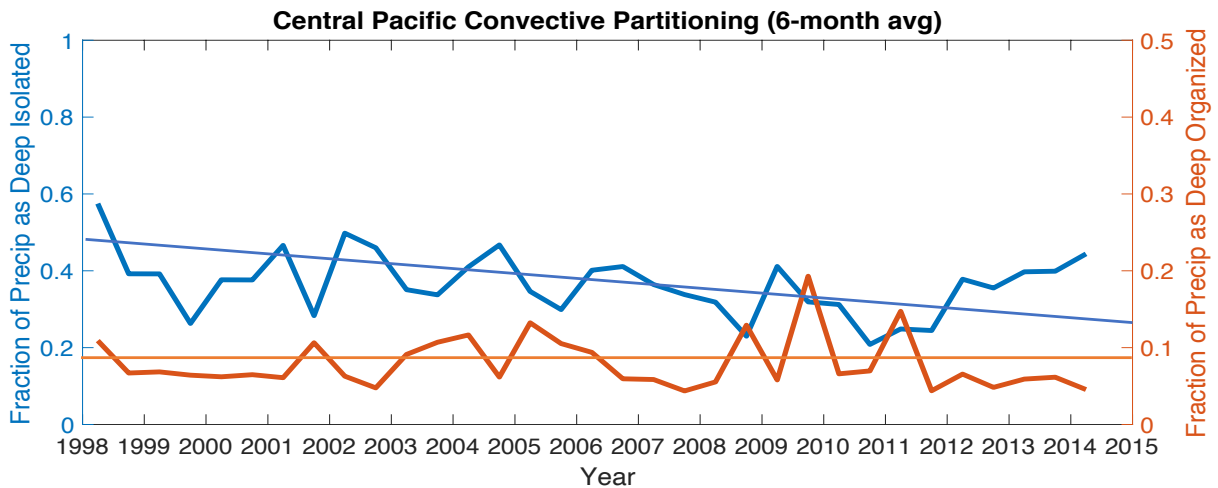


Figure 26: 6-month average of fraction of precipitation resulting from deep isolated convection and deep organized convection for the Central Pacific.

In contrast to the West Pacific pattern, the ratio between fraction of precipitation resulting from deep isolated and deep organized convection remains nearly constant throughout most of the series in all other basins. This indicates that the underestimation and overestimation by GPROF remain balanced, and the residual small. The change in ratio with time is only present in the West Pacific, supporting the hypothesis for the source of the evolving lack of closure in the West Pacific. Looking at the time series of closure magnitude shown previously in Figure 23, the evolving lack of closure appears to match the evolution of the convective partitioning fairly well when ERA-5 is used as the source for divQ. When MERRA-2 is used as the source for

divQ, the time series of closure also appears to match the evolution of convective partitioning, and the inflection point near the year 2010 is also visible.

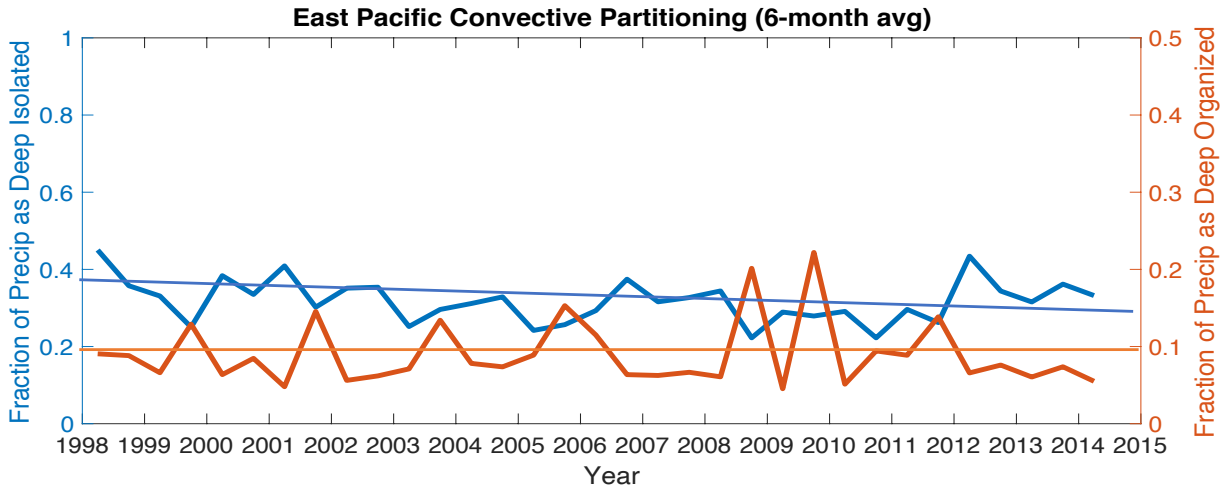


Figure 27: 6-month average of fraction of precipitation resulting from deep isolated convection and deep organized convection for the East Pacific.

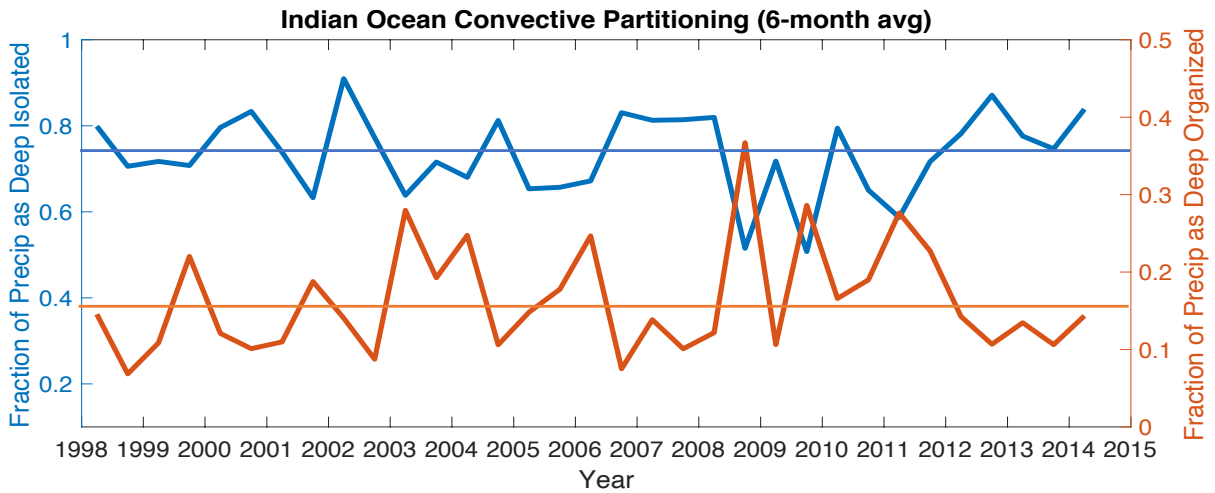


Figure 28: 6-month average of fraction of precipitation resulting from deep isolated convection and deep organized convection for the Indian Ocean.

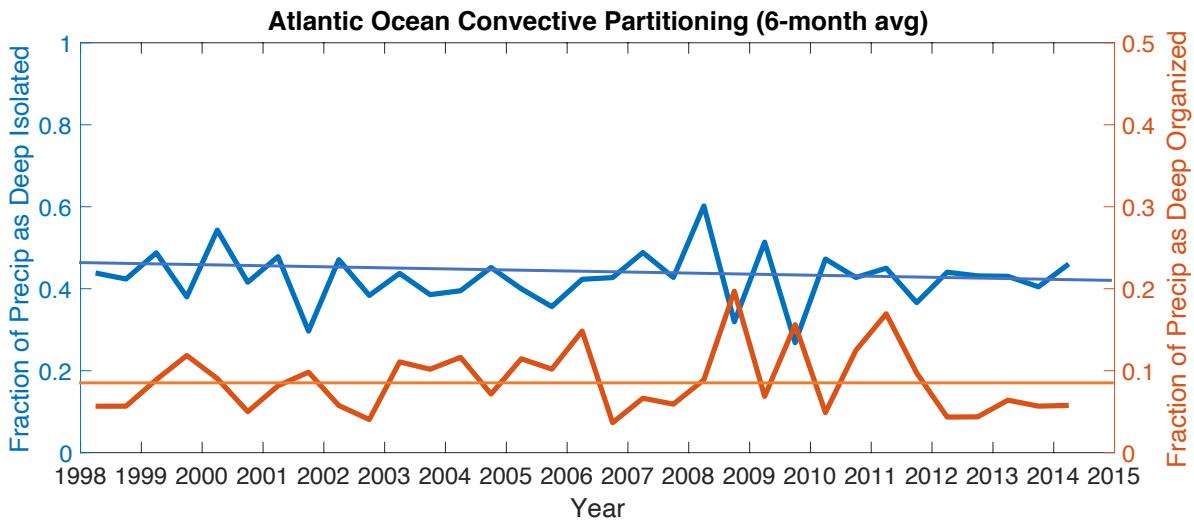


Figure 29: 6-month average of fraction of precipitation resulting from deep isolated convection and deep organized convection for the Atlantic Ocean.

This suggests that the dominating influence behind the evolving lack of closure is indeed the changing convective partitioning over time within the West Pacific region as previously hypothesized.

Based on the analysis within this work, it appears likely that the evolving lack of closure in the West Pacific is due to the aforementioned shift in the ratio between deep isolated and deep organized convective fraction limited to the West Pacific basin. A general bias in precipitation product accuracy due to fundamental changes in convective organization appears to be plausible, as the balance between the partition of isolated versus organized convection shifts with time in the West Pacific, while remaining fairly consistent in other basins. This results in an evolving lack of balance between underestimation and overestimation by the precipitation retrieval algorithms which is reflected in an evolving lack of closure in this same region.

Another coexisting trend of interest in the West Pacific is the increasing SSTs corresponding to the continual increase in the fraction of precipitation resulting from deep

isolated convection, while deep organized convection varies at the same time. This broadly suggests a connection between an increase in isolated convection corresponding to increasing SSTs in the West Pacific region. The exact physical mechanisms behind this connection between convective organization and SSTs is a topic of continued debate. Much prior work has been dedicated to understanding the exact influence of SST on convective organization and aggregation, but due to the complexity involved with modeling this relationship, as well as the sometimes competing or complimentary influences of mechanisms such as the El Nino/Southern Oscillation, the Pacific Decadal Oscillation, and the Madden-Julien Oscillation, the exact relationship still remains uncertain (Bao et al. 2017).

Several high-profile works have found that convective aggregation and organization increases with higher SSTs (e.g. Held et al. 1993, Khairoutdinov and Emanuel 2010), while other work has found that convective aggregation can still occur at low SSTs (e.g. Coppin and Bony 2015, Holloway and Woolnough 2016). This work, while generally preliminary, provides additional context in showing a relationship between increasing SSTs and increased fraction of isolated convection within which this relationship can be studied further. Ultimately, while the result of the evolving lack of closure seems to be strongly related to the evolving partitioning of deep organized and deep isolated convection, the exact environmental mechanisms behind this partitioning and why they are exclusive to the West Pacific basin still remain unknown.

Building on these conclusions, future work will incorporate a longer period of analysis as well as a larger spread of products for each variable. In addition, future work will incorporate an even more detailed and comprehensive study of the physical environment, using atmospheric and oceanic models to confirm any changes in the environment deduced from trends in the individual components of the hydrologic cycle.

REFERENCES

- Ahlgrim, M., and R. Forbes, 2013: Improving the Representation of Low Clouds and Drizzle in the ECMWF Model Based on ARM Observations from the Azores. *Monthly Weather Review*, **142**, 668-685.
- Austin, P., Wang, Y., Kujala, V., and R. Pincus, 1995: Precipitation in Stratocumulus Clouds: Observational and Modeling Results. *Journal of the Atmospheric Sciences*, **52**, 2329-2352.
- Bao, J. W., S. C. Sherwood, M. Colin, and V. Dixit, 2017: The Robust Relationship Between Extreme Precipitation and Convective Organization in Idealized Numerical Modeling Simulations. *Journal of Advances in Modeling Earth Systems*, **9**, 2291-2303.
- Brown, P. J., and C. D. Kummerow, 2014: An Assessment of Atmospheric Water Budget Components over Tropical Oceans. *Journal of Climate*, **27**, 2054-2071.
- Brunke, M. A., C. W. Fairall, X. B. Zeng, L. Eymard, and J. A. Curry, 2003: Which bulk aerodynamic algorithms are least problematic in computing ocean surface turbulent fluxes? *Journal of Climate*, **16**, 619-635.
- Chou, S. H., R. M. Atlas, C. L. Shie, and J. Ardizzone, 1995: Estimates of Surface Humidity and Latent-Heat Fluxes over Oceans from SSM/I Data. *Monthly Weather Review*, **123**, 2405-2425.
- Chou, S. H., C. L. Shie, R. M. Atlas, and J. Ardizzone, 1997: Air-sea fluxes retrieved from special sensor microwave imager data. *Journal of Geophysical Research-Oceans*, **102**, 12705-12726.
- Carr, K., and Coauthors, 2015: The Influence of Surface and Precipitation Characteristics on TRMM Microwave Imager Rainfall Retrieval Uncertainty. *Journal of Hydrometeorology*, **16**, 1596-1614.
- Chahine, M. T., 1992: The hydrological cycle and its influence on climate. *Nature*, **359**, 373-380.
- Clayson, C. A., J. B. Roberts, and A. S. Bogdanoff, 2015: The SeaFlux Turbulent Flux Dataset Version 1.0 Documentation. SeaFlux Documentation Version 1.2, 5 pp, http://seaflex.org/seaflex_data/DOCUMENTATION/SeaFluxDocumentationV12.pdf.
- Coppin, D., and S. Bony, 2015: Physical mechanisms controlling the initiation of convective self-aggregation in a General Circulation Model. *Journal of Advances in Modeling Earth Systems*, **7**, 2060-2078.
- Curry, J. A., and Coauthors, 2004: Seaflux. *Bulletin of the American Meteorological Society*, **85**, 409-424.

- Dee, D.P., and Coauthors, 2011: The ERA-Interim reanalysis: configuration and performance of the data assimilation system. *Quarterly Journal of the Royal Meteorological Society*, **137**, 553-597.
- Fairall, C. W., E. F. Bradley, J. E. Hare, A. A. Grachev, and J. B. Edson, 2003: Bulk parameterization of air-sea fluxes: Updates and verification for the COARE algorithm. *Journal of Climate*, **16**, 571-591.
- Gelaro, R., and Coauthors, 2017: The Modern-Era Retrospective Analysis for Research and Applications, Version 2 (MERRA-2). *Journal of Climate*, **30**, 5419-5454.
- Held, I. M., R. S. Hemler, and V. Ramaswamy, 1993: Radiative convective equilibrium with explicit 2-dimensional moist convection. *Journal of the Atmospheric Sciences*, **50**, 3909-3927.
- Held, I. M., and B. J. Sod, en, 2006: Robust responses of the hydrological cycle to global warming. *Journal of Climate*, **19**, 5686-5699.
- Henderson, D. S., Kummerow, C. D., Marks, D. A., and W. Berg, 2017: A Regime-Based Evaluation of TRMM Oceanic Precipitation Biases. *Journal of Atmospheric and Oceanic Technology*, **34**, 2613-2635.
- Hersbach, H., and Coauthors, 2020: The ERA5 global reanalysis. *Quarterly Journal of the Royal Meteorological Society*, **730**, 1999-2049.
- Hilburn, K. A., 2009: The passive microwave water cycle product. Remote Sensing Systems Rep. 072409, 30 pp.
- Holloway, C. E., and S. J. Woolnough, 2016: The sensitivity of convective aggregation to diabatic processes in idealized radiative-convective equilibrium simulations. *Journal of Advances in Modeling Earth Systems*, **8**, 166-195.
- Hong, Y., K. L. Hsu, S. Sorooshian, and X. G. Gao, 2004: Precipitation Estimation from Remotely Sensed Imagery using an Artificial Neural Network Cloud Classification System. *Journal of Applied Meteorology*, **43**, 1834-1852.
- Hou, A. Y., and Coauthors, 2014: The Global Precipitation Measurement Mission. *Bulletin of the American Meteorological Society*, **95**, 701-722.
- Joyce, R., and P. Xie, 2011: Kalman Filter-Based CMORPH. *Journal of Hydrometeorology*, **12**, 1547-1563.
- Khairoutdinov, M. F., and K. A. Emanuel, 2010: Aggregated Convection and the Regulation of Tropical Climate. *29th Conference on Hurricanes and Tropical Meteorology*, Tucson, AZ, American Meteorological Society, P2.69.

- Kummerow, C., Barnes, W., Kozu, T., Shiue, J., and J. Simpson, 1998: The Tropical Rainfall Measurement Mission (TRMM) Sensor Package. *Journal of Atmospheric and Oceanic Technology*, **15**, 809-817.
- Kummerow, C. D., Ringerud, S., Crook, J., Randel, D., and W. Berg, 2011: An Observationally Generated A Priori Database for Microwave Rainfall Retrievals. *Journal of Atmospheric and Oceanic Technology*, **28**, 113-130.
- Kummerow, C. D., D. L. Randel, M. Kulie, N. Wang, R. Ferraro, S. J. Munchak, and V. Petkovic, 2015: The evolution of the Goddard profiling algorithm to a fully parametric scheme. *Journal of Atmospheric and Oceanic Technology*, **32**, 2265–2280.
- L'Ecuyer, T. S., and Coauthors, 2015: The Observed State of the Energy Budget in the Early Twenty-First Century. *Journal of Climate*, **28**, 8319-8346.
- Leese, J. A., Novak, C. S., and B. B. Clark, 1971: An automated technique for obtaining cloud motion from geosynchronous satellite data using cross correlation. *Journal of Applied Meteorology*, **10**, 118-132.
- Randel, D. L., Kummerow, C. D., and S. Ringerud, 2015: The Goddard Profiling (GPROF) Precipitation Retrieval Algorithm, *Satellite Precipitation Measurement, Vol. 1*, V. Levizzani, C. Kidd, D. B. Kirschbaum, C. D. Kummerow, K. Nakamura, F. J. Turk, Ed., Springer, 141-152.
- Rasmusson, E. M., 1967: Atmospheric water vapor transport and the water balance of North America, Part 1. Characteristics of the water vapor flux field. *Monthly Weather Review*, **96**, 720-734.
- Rasmusson, E. M., 1977: Hydrological application of atmospheric vapor-flux analysis. *Operational Hydrology Report 11*, World Meteorological Organization.
- Reynolds, R. W., T. M. Smith, C. Liu, D. B. Chelton, K. S. Casey, and M. G. Schlax, 2007: Daily high-resolution-blended analyses for sea surface temperature. *Journal of Climate*, **20**, 5473-5496.
- Rienecker, M. M., and Coauthors, 2011: MERRA: NASA's Modern-Era Retrospective Analysis for Research and Applications. *Journal of Climate*, **24**, 3624-3648.
- Roberts, J. B., C. A. Clayson, F. R. Robertson, and D. L. Jackson, 2010: Predicting near-surface atmospheric variables from Special Sensor Microwave/Imager using neural networks with a first-guess approach. *Journal of Geophysical Research-Atmospheres*, **115**.
- Roberts, J. B., F. R. Robertson, C. A. Clayson, and M. G. Bosilovich, 2012: Characterization of Turbulent Latent and Sensible Heat Flux Exchange between the Atmosphere and Ocean in MERRA. *Journal of Climate*, **25**, 821-838.
- Rodell, M., and Coauthors, 2015: The Observed State of the Energy Budget in the Early Twenty-First Century. *Journal of Climate*, **28**, 8289-8318.

- Sherwood, S. C., Lanzante, J. R., and C. L. Meyer, 2005: Radiosonde daytime biases and late-20th century warming. *Science*, **309**, 1556-1559.
- Stephens, G. L., and Coauthors, 2010: Dreary state of precipitation in global models. *Journal of Geophysical Research-Atmospheres*, **115**.
- Stephens, G. L., and Coauthors, 2012: An update on Earth's energy balance in light of the latest global observations. *Nature Geoscience*, **5**, 691-696.
- Trenberth, K. E, J. T. Fasullo, and J. Kiehl, 2009: Earth's Global Energy Balance. *Bulletin of the American Meteorological Society*, **90**, 311-323.
- Wild, M., D. Folini, C. Schar, N. Loeb, E. G. Dutton, and G. Konig-Langlo, 2013: The global energy balance from a surface perspective. *Climate Dynamics*, **40**, 3107-3134.
- Wilheit, T. T., Chang, A. T. C., Rao, M. S. V., Rodgers, E. B., and J. S. Theon, 1977: A satellite technique for quantitatively mapping rainfall rates over the ocean. *Journal of Applied Meteorology*, **16**, 551-560.
- Wilheit, T. T., and A. T. C. Chang, 1980: An algorithm for retrieval of ocean surface and atmospheric parameters from the observations of the scanning multichannel microwave radiometer. *Radio Science*, **15**, 525-544.
- Wilheit, T. T., A. T. C. Chang, and L. S. Chiu, 1991: Retrieval of monthly rainfall indexes from microwave radiometric measurements using probability-distribution functions. *Journal of Atmospheric and Oceanic Technology*, **8**, 118-136.
- Xie, X., Liu, W. T., and B. Tang, 2008: Space-based estimation of moisture transport in marine atmosphere using support vector regression. *Remote Sensing of Environment*, **112**, 1845-1855.
- Young, M. T., Doolittle, R. C., and L. M. Mace, 1972: Operational procedures for estimating wind vectors from geostationary satellite data. *NOAA Technical Memorandum NESS 39*.
- Yu, L. S., 2019: Global Air-Sea Fluxes of Heat, Fresh Water, and Momentum: Energy Budget Closure and Unanswered Questions. *Annual Review of Marine Science, Vol 11*, **11**, 227-248.
- Yu, L. S., and R. A. Weller, 2007: Objectively analyzed air-sea heat fluxes for the global ice-free oceans (1981-2005). *Bulletin of the American Meteorological Society*, **88**, 527-540.
- Yu, L. S., X. Jin, and R.A. Weller, 2008: Multidecade Global Flux Datasets from the Objectively Analyzes Air-sea Fluxes (OAFlux) Project: Latent and Sensible Heat Fluxes, Ocean Evaporation, and Related Surface Meteorological Variables. Woods Hole Oceanographic Institution OAFlux Project Technical Report OA-2008-01, 64 pp, http://oaflux.whoi.edu/pdfs/OAFlux_TechReport_3rd_release.pdf.